Phosphoglycerate mutase regulates Treg differentiation through control of serine synthesis and one-carbon metabolism

Wesley H. Godfrey[1], Judy J. Lee[1], Shruthi Shanmukha[2], Kaho Cho[1], Xiaojing Deng[1], Chandra Shekar R. Ambati[3], Vasanta Putluri[3], Abu Hena Mostafa Kamal[3,4], Paul M. Kim[2], Nagireddy Putluri[3,4], and Michael D. Kornberg[1*]

[1]Department of Neurology, Johns Hopkins University School of Medicine, Baltimore, Maryland 21287, USA

[2]Department of Psychiatry and Behavioral Sciences, Johns Hopkins University School of Medicine, Baltimore, Maryland 21287, USA

[3]Advanced Technology Core, Baylor College of Medicine, Houston, TX 77030, USA.

[4]Department of Molecular and Cellular Biology, Baylor College of Medicine, Houston, TX 77030, USA.

*Corresponding Author: michael.kornberg@jhmi.edu

Abstract

The differentiation and suppressive functions of regulatory CD4 T cells (Tregs) are supported by a broad array of metabolic changes, providing potential therapeutic targets for immune modulation. In this study, we focused on the regulatory role of glycolytic enzymes in Tregs and identified phosphoglycerate mutase (PGAM) as being differentially overexpressed in Tregs and associated with a highly suppressive phenotype. Pharmacologic or genetic inhibition of PGAM reduced Treg differentiation and suppressive function while reciprocally inducing markers of a pro-inflammatory, T helper 17 (Th17)-like state. The regulatory role of PGAM was dependent on the contribution of 3-phosphoglycerate (3PG), the PGAM substrate, to de novo serine synthesis. Blocking de novo serine synthesis from 3PG reversed the effect of PGAM inhibition on Treg polarization, while exogenous serine directly inhibited Treg polarization. Additionally, altering serine levels *in vivo* with a serine/glycine-free diet increased peripheral Tregs and attenuated autoimmunity in a murine model of multiple sclerosis. Mechanistically, we found that serine limits Treg polarization by contributing to one-carbon metabolism and methylation of Treg-associated genes. Inhibiting one-carbon metabolism increased Treg polarization and suppressive function both *in vitro* and *in vivo* in a murine model of autoimmune colitis. Our study identifies a novel physiologic role for PGAM and highlights the metabolic interconnectivity between glycolysis, serine synthesis, one-carbon metabolism, and epigenetic regulation of Treg differentiation and suppressive function.

Introduction

Upon activation, immune cells undergo drastic metabolic changes that support their differentiation and effector functions. The regulation of immune responses by metabolic pathways, termed “immunometabolism”, has become a major focus of research with a goal of identifying pathways that can be targeted in conditions ranging from autoimmune and infectious diseases to cancer[1].

T lymphocytes in particular have emerged as a central focus of immunometabolic research with far reaching implications in human disease [2–7]. Among the metabolic adaptations associated with T cell activation, glycolytic reprogramming plays a prominent role. Increased glucose uptake and augmented glycolysis are critical for the differentiation and effector functions of inflammatory T cell subsets, including effector CD8 cells and T-helper (Th) 1 and Th17 CD4 cells [8–15]. In contrast, regulatory T cells (Tregs), which serve as the brakes of the immune response by promoting tolerance and suppressing inflammation, have a distinct glycolytic profile [16,17]. Prior work has shown that initial engagement of glycolysis supports proliferation and migration of Tregs, whereas downregulation of glycolysis and greater engagement of fatty acid oxidation are required for expression of the Treg-specific transcription factor FOXP3 and Treg suppressive functions[18–25]. In this regard, forced engagement of glycolysis was found to decrease FOXP3 expression [26] while inhibition of glycolysis favored Treg differentiation and suppressive functions [15,25,27–29]. The relationship between glycolysis and Treg function is not straightforward, however. For instance, in human Tregs induced following weak stimulation of the T cell receptor (TCR), glycolysis supported Treg suppressive function by regulating DNA-binding activity of the glycolytic enzyme enolase-1 (ENO1) [30]. Such findings suggest the possibility of a more nuanced role for glycolysis in Tregs, with individual glycolytic enzymes serving unique and perhaps disparate functions.

Here, we report that the glycolytic enzyme phosphoglycerate mutase (PGAM), which converts 3-phosphoglycerate (3PG) to 2-phosphoglycerate (2PG), is physiologically upregulated in Tregs and its enzymatic activity supports FOXP3 expression and Treg suppressive function. Pharmacologic or genetic inhibition of PGAM inhibited Treg differentiation and shifted CD4 T cells toward a pro-inflammatory, Th17-like state. Mechanistically, we found that PGAM regulates Treg differentiation by controlling flux through the de novo serine synthesis pathway. The PGAM substrate 3PG is also utilized for serine synthesis, and decreased PGAM enzyme activity led to increased serine synthesis through accumulation of 3PG. Both newly synthesized and imported extracellular serine inhibited Treg differentiation by contributing to one-carbon metabolism and promoting the methylation, and therefore silencing, of genes associated with Treg function. Manipulation of serine availability and the methylation cycle increased peripheral Tregs and attenuated disease in mouse models of multiple sclerosis and autoimmune colitis. Our finding that PGAM, a key glycolytic enzyme, physiologically supports Treg differentiation further challenges the notion that glycolysis plays a singular, inhibitory role in Tregs and

suggests that individual glycolytic enzymes can serve as nodes for the fine-tuning of immune responses. Furthermore, our work identifies novel metabolic targets for the therapeutic manipulation of Treg function in human disease.

Results

PGAM regulates Treg differentiation and suppressive function

In order to identify the glycolytic enzymes that play the largest role in Treg differentiation, we analyzed multiple publicly available transcriptomic and proteomic datasets. We first investigated an RNA sequencing (RNA-seq) dataset that compared human naïve CD4 cells cultured under either Th0 or Treg polarizing conditions [31]. After library normalization, we examined genes included in the "Glycolysis and Gluconeogenesis" gene ontology (GO) term and found that *PGAM1* was the most differentially expressed glycolytic gene, with upregulation in *in vitro*-induced Tregs (iTregs) compared to conventional Th0 cells (Figure 1A). To determine whether PGAM expression is similarly upregulated in ex vivo-derived Tregs, we examined a single cell RNA-seq (scRNA-seq) dataset of peripheral blood mononuclear cells (PBMCs) from human healthy controls [32] and compared glycolytic gene expression between Tregs and total CD4 cells. After removing glyceraldehyde-3-phosphate dehydrogenase (*GAPDH*) for scaling purposes, we found that *PGAM1* was similarly upregulated in Tregs (Figure 1B). A proteomics dataset from human healthy donor PBMCs [33] demonstrated significantly upregulated protein levels of PGAM1 and PGAM2 in Tregs compared to total CD4 cells (Figure 1C), confirming findings from the mRNA level.

The differential upregulation of PGAM in Tregs suggested that it might play a physiologic regulatory role in these cells. We therefore wondered whether PGAM inhibition impacts Treg differentiation. To answer this question, we used epigallocatechin gallate (EGCG), a known inhibitor of PGAM [34]. We cultured naïve murine CD4 cells under Treg polarizing conditions with either vehicle (solvent alone) or EGCG and assessed Treg differentiation by quantifying the percentage of $CD25^{+}FOXP3^{+}$ cells by flow cytometry after 96 hours. Treatment with EGCG significantly reduced Treg differentiation (Figure 1D) without affecting proliferation or cell viability (Figure S1). To validate the effects of pharmacologic inhibition with genetic knockdown, we utilized antisense oligonucleotides (ASOs) targeting PGAM to reduce gene expression. Experiments conducted with fluorescently-tagged ASOs demonstrated near-complete ASO uptake by cultured CD4 cells after 24 hours (Figure S2). Compared to scrambled control ASOs, we found that ASOs targeting PGAM reduced PGAM1 protein levels (Figure S3A) and significantly reduced Treg differentiation assessed by flow cytometry (Figure 1E). Because glycolysis is crucial for cell health, we wanted to know if PGAM knockdown was affecting survival and/or proliferation. We found that PGAM ASOs did not affect cell survival and led to a minor increase in cell proliferation (Figures S3B and S3C).

To gain further insights into the effects of PGAM knockdown on Treg differentiation, we performed RNA-seq transcriptional profiling from unsorted naïve murine CD4 cells cultured under Treg polarizing conditions with either scrambled or PGAM-specific ASOs. PCA analysis showed that PGAM ASOs led to major transcriptional changes (Figure 1F), with major effects on MYC targets and mTORC1 signaling (Figure 1G), among other changes. We then performed differential expression analysis on a subset of genes important in the Treg-Th17 axis and found that cells treated with PGAM ASOs had significantly higher expression of pro-inflammatory genes such as *Il17*, *Il22*, and *Il9*, while significantly lower expression of genes involved in Treg differentiation such as *Foxp3* and *Izkf3* (Figure 1H). A complete list of differentially expressed genes can be found in Table S1.

Given the observed changes in transcriptional profile and differentiation markers, we next asked whether PGAM knockdown leads to functional changes in Treg suppressive activity. Compared to treatment with scrambled ASOs, PGAM ASO-treated Tregs were less effective at suppressing effector T (Teff) cell proliferation, indicating diminished suppressive function (Figure 1I). To determine whether PGAM expression is associated with Treg suppressive activity in human disease, we examined a published scRNAseq dataset of tumor-infiltrating Tregs (TIL-Tregs) isolated from surgically resected non-small cell lung cancer [35]. Among the 10 distinct subsets of TIL-Tregs identified in this study, one subset, the $OX40^{hi}GITR^{hi}$ cluster [termed "Activated (1)" by the authors] had markedly increased suppressive activity and was enriched in

patients who were resistant to immune checkpoint blockade. Strikingly, *PGAM1* was significantly overexpressed in the highly suppressive OX40^{hi}GITR^{hi} cluster compared to the 9 other TIL-Treg subsets (Figure 1J). Moreover, *PGAM1* expression was selectively increased in this subset relative to proximal, rate-limiting glycolytic enzymes, suggesting a unique association between PGAM expression and Treg suppressive activity.

Taken together, these findings demonstrate a critical role for PGAM in promoting Treg differentiation and suppressive function, *in vitro* as well as in healthy and diseased human states. The positive regulatory role of PGAM in Tregs was intriguing, since glycolysis has generally been associated with decreased Treg function. Indeed, whereas inhibition or knockdown of PGAM led to decreased Treg differentiation, our own prior work found that similar inhibition of GAPDH, which catalyzes a reaction only two steps upstream from PGAM in glycolysis, had the opposite effect[28] – a finding we replicated here with the GAPDH inhibitor koningic acid (Figure S4). Consistent with this observation, the ratio of *PGAM1* to *GAPDH* mRNA levels increased in human iTregs vs. Th0 cells (Figure S5A), and PGAM2 protein levels increased out of proportion to GAPDH (and other glycolytic enzymes) in ex vivo Tregs (Figure 1C). Similarly, a review of published data from the ImmPres immunological proteome resource (http://immpres.co.uk/)[36] shows increased PGAM1/GAPDH protein copy number ratio in murine iTregs versus Th17 cells (Figure S5B), further implicating a specific role for PGAM in the Treg-Th17 axis. The discordant roles of GAPDH and PGAM in Tregs led us to focus on the glycolytic metabolites downstream of GAPDH and upstream of PGAM, as the concentrations of these metabolites would be differentially impacted by the two enzymes (Figure 2A).

PGAM regulation of Treg differentiation is mediated by 3PG and de novo serine synthesis

PGAM metabolizes the glycolytic intermediate 3PG into 2PG [37,38]. In addition to its role in glycolysis, 3PG is the starting substrate for the de novo serine synthesis pathway [39,40]. Given previous work implicating various roles for serine in T cells [41–43], we hypothesized that PGAM enzymatic activity regulates Treg differentiation and function by controlling levels of 3PG with downstream effects on serine synthesis (Figure 2A). To test this hypothesis, we first cultured naïve murine CD4 cells under Treg-polarizing conditions with either vehicle or the PGAM inhibitor EGCG and measured intracellular serine levels from unsorted cells by mass spectrometry. As anticipated, PGAM inhibition with EGCG increased intracellular levels of serine in Tregs (Figure 2B). We next asked whether glucose-derived de novo serine synthesis is physiologically regulated during Treg differentiation, focusing on the reciprocal Treg-Th17 axis. Following incubation with uniformly 13-carbon labeled glucose (U^{13}C-glucose), serine that is newly synthesized from 3PG has a mass-shift of 3 (M+3) when analyzed by mass spectrometry, whereas unlabeled, non-glucose-derived serine has no mass-shift (M+0). We differentiated naïve murine CD4 cells into either Tregs or Th17 cells for 72 hours. After 6-hour glucose starvation, the cells were incubated with U^{13}C-glucose for an additional 6 hours. Using mass spectrometry, we found that ^{13}C-labeling of serine was significantly higher in Th17 cells compared to Tregs (Figure 2C), indicating that flux through de novo serine synthesis is physiologically downregulated in Tregs compared to Th17 cells. Because serine can be recycled via one-carbon metabolism, we observed an increase in one carbon-labeled (M+1) serine as well as M+3 serine in Th17 cells relative to Treg cells.

If the role of PGAM in Treg differentiation depends on de novo serine synthesis, then the effects of PGAM inhibition should be rescued by simultaneously blocking the serine synthesis pathway. To this end, we cultured naïve murine CD4 cells under Treg-polarizing conditions and treated them with the PGAM inhibitor EGCG ± NCT-503, an inhibitor of phosphoglycerate dehydrogenase (PHGDH, the rate-limiting enzyme of serine synthesis from 3PG) [44,45]. As before, PGAM inhibition with EGCG inhibited Treg differentiation as assessed by FOXP3 expression, but this was reversed by PHGDH inhibition with NCT-503 (Figure 2D). Similarly, if PGAM regulates Tregs by controlling concentrations of 3PG (the substrate for serine synthesis), then direct supplementation of 3PG should replicate the effects of PGAM inhibition. To test this, 3PG was delivered to naïve murine CD4 cells via electroporation followed by Treg polarization. As expected, 3PG supplementation decreased FOXP3 expression, which was rescued by PHGDH inhibition with NCT-503 (Figure 2E). To further validate the role of de novo serine synthesis in Tregs, we used PHGDH-targeted ASOs and found that genetic knockdown of PHGDH led to augmented Treg differentiation as assessed by FOXP3 expression (Figure 2F).

The above findings demonstrate that PGAM regulates Treg differentiation by controlling flux through the serine synthesis pathway. Because serine can be derived from both de novo intracellular synthesis and extracellular sources, we next asked whether extracellular serine also affects Treg differentiation. We cultured naïve murine CD4 cells under Treg-polarizing conditions in either serine/glycine-free media or serine/glycine-free media supplemented with 4 mM serine. Deprivation of both serine and glycine is required to evaluate the role of extracellular serine, as glycine can be converted to serine via the enzyme serine hydroxymethyltransferase (SHMT)[40]. The presence of extracellular serine diminished Treg differentiation (Figure 2G), indicating that both synthesized and exogenous serine impact Treg generation.

Synthesized and dietary serine regulate Treg function in vivo

After finding that serine derived from both extracellular sources and de novo synthesis inhibits Treg polarization *in vitro*, we investigated the effect on Tregs of altering serine availability *in vivo*. We first examined the impact of dietary serine restriction by maintaining mice immediately post-weaning on either a serine/glycine-free diet or isocaloric control diet. After 8 weeks, we measured Treg abundance in peripheral blood by flow cytometry. Mice fed a serine/glycine-free diet had significantly higher proportions of Tregs in peripheral blood (Figure 3A). To determine whether this effect on Tregs translates to protection in a murine model of autoimmunity, we used the myelin oligodendrocyte glycoprotein $(MOG)_{35-55}$ experimental autoimmune encephalomyelitis (EAE) model of multiple sclerosis (MS). Mice were transitioned to a serine/glycine-free or isocaloric control diet beginning one week prior to immunization with MOG_{35-55}, and disease severity was monitored by a blinded scorer. A serine/glycine-free diet significantly attenuated disease severity, delaying the onset of neurologic deficits and reducing peak clinical scores (Figures 3B-D).

We next asked whether de novo serine synthesis is altered in human Tregs in disease. Using publicly available RNA-seq and scRNA-seq data, we estimated the rate of de novo serine synthesis using single cell flux estimation analysis (SCFEA)[46], which constructs a global set of metabolic reactions as a factor map and uses multi-layer neural networks to model reaction rates from mRNA levels of metabolic enzymes. We applied SCFEA to human Th0 and iTreg cells differentiated from naïve CD4 cells *in vitro*[31] and found that serine synthesis was downregulated in iTregs (Figure 3E). Autoimmunity occurs when Tregs fail to adequately regulate the immune response, so we wondered whether the predicted rate of de novo serine synthesis would be altered in Tregs derived from patients with autoimmune disease. Using scRNA-seq data derived from Tregs isolated from the cerebrospinal fluid (CSF) of patients with treatment-naïve relapsing MS and controls [32], we found the predicted rate of serine synthesis was significantly higher in Tregs from MS patients (Figure 3F). Conversely, while autoimmunity results from inadequate Treg suppressive function, Tregs in the tumor microenvironment have pathologically high suppressive function. We examined scRNA-seq data from Tregs derived from healthy prostate and prostate cancer [47] from the IMMUcan database [48] and found that prostate tumor-infiltrating Tregs had significantly lower predicted serine synthesis than Tregs from healthy prostate (Figure 3G). Consistent with our earlier findings that serine synthesis inhibits Treg function, these analyses suggest that serine synthesis within Tregs is higher in autoimmunity and lower in the tumor microenvironment, thereby negatively correlating with expected Treg suppressive function in human disease.

Serine inhibits Treg generation by contributing to one-carbon metabolism and DNA methylation

We next examined the mechanistic links between serine metabolism and Treg function. Serine can serve as a one-carbon donor by entering the one-carbon metabolism cycle, which depends on conversion into glycine by the enzyme SHMT1/2 [49] (Figure 4A). To determine whether the effects of serine on Treg differentiation depend on contributions to one-carbon metabolism, we cultured naïve murine CD4 cells under Treg polarizing conditions with either vehicle or the SHMT1/2 inhibitor SHIN1[50,51]. Inhibiting SHMT1/2 increased Treg polarization (Figure 4B) and mitigated the inhibitory effect of extracellular serine on Tregs (Figure 4C). Because methionine can compensate as a one-carbon donor, other groups have found that the contribution of serine to one-carbon metabolism is greater in the absence of methionine[52]. To further the idea that serine inhibits Treg polarization by contributing to one-carbon metabolism, we cultured naïve murine CD4 cells under Treg polarizing conditions in methionine-free media supplemented with either methionine or excess serine. Although methionine supplementation had little effect in the presence of physiologic extracellular serine

(0.4 mM), excess extracellular serine (4 mM) was highly potent in inhibiting Treg polarization in the absence of methionine (Figure 4D). These studies suggest that the regulatory role of serine in Tregs is mediated at least in part through one-carbon metabolism.

A crucial role of one-carbon metabolism is to provide methyl groups for methylation reactions, and DNA methylation represents a key epigenetic mechanism used to silence gene transcription[53]. We therefore asked whether serine entry into one-carbon metabolism contributes to DNA methylation in Tregs, so we conducted a carbon tracing experiment in which Tregs were cultured in media containing uniformly 13-carbon labeled serine ($U^{13}C$-serine) for 12 hours before DNA was isolated from the unsorted cells and analyzed by mass spectrometry. We found that serine directly contributed to cytosine methylation, as measured by carbon labeling of methylcytosine (Figure 4E). Demethylation of the Treg-specific demethylated region (TSDR) in Tregs is a critical step for generation of stable, bona fide Tregs, and methylation in this region is associated with transient or unstable expression of FOXP3 and suppressive activity [54]. We therefore investigated the effects of extracellular serine and PGAM knockdown on methylation of the TSDR via pyrosequencing. In a first set of experiments, naïve murine CD4 cells were cultured under Treg polarizing conditions in either serine/glycine-free media or media containing serine. The presence of extracellular serine increased TSDR methylation (Figure 4F). Genetic knockdown of PGAM using ASOs similarly increased TSDR methylation (Figure 4G). Taken together, these findings demonstrate that both extracellular serine and PGAM-regulated serine synthesis increase the methylation, and therefore silencing, of Treg-associated genes.

Given the promising results seen with pyrosequencing, we next used a next generation sequencing panel to identify CpG sites in Treg-specific genes whose methylation is regulated by serine (Figure 4H). Methylation of *Ikzf2* (Helios) was significantly increased with the addition of extracellular serine, but this was reversed by blocking serine entry into one-carbon metabolism with the SHMT inhibitor SHIN1. In the 5' upstream region of the *Foxp3* gene, one CpG site showed significantly higher methylation in the presence of serine, and this effect was reversed by SHIN1. A complete list of CpG methylation levels can be found in Table S2.

To definitively link methylation to Treg differentiation and suppressive function, we blocked methylation in Tregs with 3-Deazaadenosine (3DZA), an inhibitor of S-adenosylhomocysteine (SAH) hydrolase. SAH hydrolase degrades SAH and prevents recycling of the methyl donor S-adenosylmethionine (SAM) [55]. In naïve murine CD4 cells cultured under Treg polarizing conditions, 3DZA increased Treg differentiation (Figure 4I) without affecting cell viability (Figure S6). Treatment with 3DZA similarly augmented suppressive function in cultured murine Tregs (Figure 4J). To determine the *in vivo* relevance of these findings, we used an adoptive transfer RAG colitis mouse model. Conventional murine CD4 cells were activated ex vivo and injected into $RAG^{-/-}$ mice to induce colitis, along with simultaneous injection of Tregs that had been treated during differentiation with either vehicle or 3DZA. Mice injected with Tregs polarized in the presence of 3DZA had less severe disease as measured by weight loss and colonic damage (Figures 4K and S7), indicating greater Treg suppressive function. Altogether, these findings demonstrate that one-carbon metabolism and methylation impair Treg differentiation and suppressive function both *in vitro* and *in vivo*.

Discussion

In this study, we found that PGAM plays a key physiologic role in Treg differentiation and suppressive function through regulation of serine synthesis, which intersects with glycolysis immediately upstream of PGAM through the shared substrate 3PG. Analysis of published datasets revealed that PGAM expression is specifically increased within human Tregs at both transcriptional and protein levels, and further that PGAM expression is enriched in highly suppressive Treg phenotypes. Pharmacologic inhibition or genetic knockdown of PGAM reduced Treg polarization and suppressive function while promoting a pro-inflammatory gene signature. These effects were replicated by exogenous supplementation of 3PG and reversed by inhibition of serine synthesis. Single cell flux estimation analysis predicted increased serine synthesis in Tregs isolated from patients suffering from autoimmune disease and decreased serine flux in tumor-associated Tregs, underlining the clinical importance of this regulatory pathway. Consistent with a previous report [43], we found that both synthesized and exogenously imported serine impact Treg function. Mechanistically, serine inhibited Treg

polarization by increasing flux through one-carbon metabolism with downstream effects on DNA methylation of Treg-related genes. Interfering with serine availability or methylation attenuated disease in *in vivo* models of autoimmunity.

The surprising role of PGAM in Treg differentiation has both physiologic and therapeutic implications. Although glycolysis has been shown to support initial proliferation and migration of Tregs[21,30], most prior work has suggested that glycolytic flux supports effector T cell functions with concomitant downregulation of Treg stability and suppressive activity[29,56–58]. Indeed, previous studies have shown Tregs to depend on fatty acid oxidation and oxidative phosphorylation, largely independent of glycolysis[17,59,60]. Our own prior work found that inhibition of GAPDH, an enzyme two catalytic reactions upstream of PGAM in glycolysis, enhances Treg differentiation[28], with similar findings observed following inhibition or knockdown of other proximal glycolytic enzymes[15,22,27,61]. It is striking, therefore, that PGAM enzymatic activity has the opposite effect. Inhibition or knockdown of PGAM not only attenuated Treg differentiation and suppressive function but reciprocally enhanced markers of a pro-inflammatory, Th17-like phenotype, implicating PGAM as a physiologic regulator of the balance between pro- and anti-inflammatory lymphocyte responses via regulation of serine synthesis. These findings suggest that glycolytic regulation of immunity is more complex than previously appreciated, supporting a more granular view in which glycolytic enzymes can serve as independent regulatory nodes for the fine-tuning of immune responses. Our data suggest that these differential effects of glycolytic enzymes might be mediated by fine control of the metabolites whose concentrations they regulate, such as 3PG in the case of PGAM.

From a therapeutic perspective, our findings identify novel targets for modulating Treg function in disease. Substantial prior work has shown that manipulation of glycolysis and other metabolic pathways has a therapeutic window for systemic administration despite the ubiquity of these pathways in cell biology [62]. Nonetheless, systemic administration may not be necessary for several key therapeutic applications, for instance optimization of chimeric antigen receptor (CAR)-T cell therapies[63–65]. Differentiation of CAR-T cells into a Treg-like state correlates with failure of CAR-T therapy in B cell lymphoma [66], such that manipulation of PGAM and downstream serine metabolism and DNA methylation is a potential strategy for improving the anti-cancer fitness of CAR-T cells *ex vivo* prior to infusion. Conversely, CAR-Tregs are currently in clinical trials for a variety of autoimmune disorders[67,68], and there is widespread interest in treatments that improve the suppressive activity of Tregs.

Of note, a prior study reported that complete knockout of PGAM1 in T cells impaired differentiation and effector functions of pro-inflammatory T cell subsets with only mild impact on Treg generation[69]. However, complete knockout of a glycolytic enzyme would be expected to abrogate glycolytic flux entirely, with wide-ranging effects (including decreased energy production) likely to mask the impact of physiologic or therapeutic modulation of enzyme function. As we showed here, partial knockdown or pharmacologic inhibition of PGAM1, which decreases but does not fully abrogate enzymatic activity, substantially reduced Treg differentiation while supporting pro-inflammatory activation. Additionally, other groups studying glycolysis in cancer used partial knockdowns to show that PGAM supports tumor proliferation by controlling flux through the de novo serine synthesis pathway[70].

Our investigation focused on the contribution of one-carbon metabolism to DNA methylation, which is particularly relevant in Tregs given the established regulatory role of methylation of Treg-specific genes, including the Treg Specific Demethylated Region (TSDR) of the FOXP3 gene locus[71–74]. However, one-carbon metabolism contributes to many cellular processes, including purine synthesis, amino acid metabolism, and phospholipid synthesis, among others [53], so it is likely that one-carbon metabolism inhibits Treg differentiation in a variety of ways. Although other groups have also identified the importance of one-carbon metabolism in Treg generation[75], we describe novel links between glycolysis, serine synthesis, and DNA methylation as a regulatory pathway of Treg differentiation.

In summary, we have found an unexpected role of PGAM that adds further nuance to the complex relationship between glycolysis and Treg function and further implicates serine and its contributions to one-carbon metabolism and DNA methylation as key regulators of Treg differentiation. In addition to yielding new biological insights into the metabolic regulation of lymphocyte fate and function, these findings point to new strategies for the therapeutic manipulation of Treg function.

Acknowledgments

We kindly thank Matthew Smith, Payam Gharibani, Erika Pearce, Ed Pearce, Brett Morrison, and Peter Calabresi for constructive comments and technical assistance. Additionally, we thank EpigenDx for their help with methylation NGS panels and pyrosequencing. Figures 2A and 4A were made using Biorender.com.

This work was supported by NIH/NINDS Grant K08NS104266, Conrad N. Hilton Foundation Marilyn Hilton Bridging Award for Physician Scientists Grant 17316, and a Herbert R. and Jeanne C. Mayer Foundation grant to MDK. WHG was supported by NIH MSTP Grant T32 GM136577 and a Careers in Immunology Fellowship Award from the American Association of Immunologists. Metabolomics and mass spectrometry work was supported by the following awards to NP: CPRIT Proteomics and Metabolomics Core Facility (RP210227), NIH (P30 CA125123), NIH (R01CA282282) and Dan L. Duncan Cancer Center.

Author Contributions

Conceptualization, WHG and MDK; Investigation, WHG, JJL, SS, XD, KC (General); CA, VP, AHMK (Mass Spectrometry); Formal Analysis, WHG, JJL, MDK (General); VP, AHMK, NP (Mass Spectrometry); Writing – Original Draft, WHG and MDK; Writing – Review & Editing, WHG, MDK, NP; Supervision, PMK, NP, MDK; Funding Acquisition, NP and MDK.

Declaration of Interests

MDK has received ad hoc consulting fees from Biogen Idec, Genentech, Janssen Pharmaceuticals, Novartis, OptumRx, and TG Therapeutics on topics unrelated to this manuscript. The remaining authors declare that the research was conducted in the absence of any commercial or financial relationships that could be construed as a potential conflict of interest.

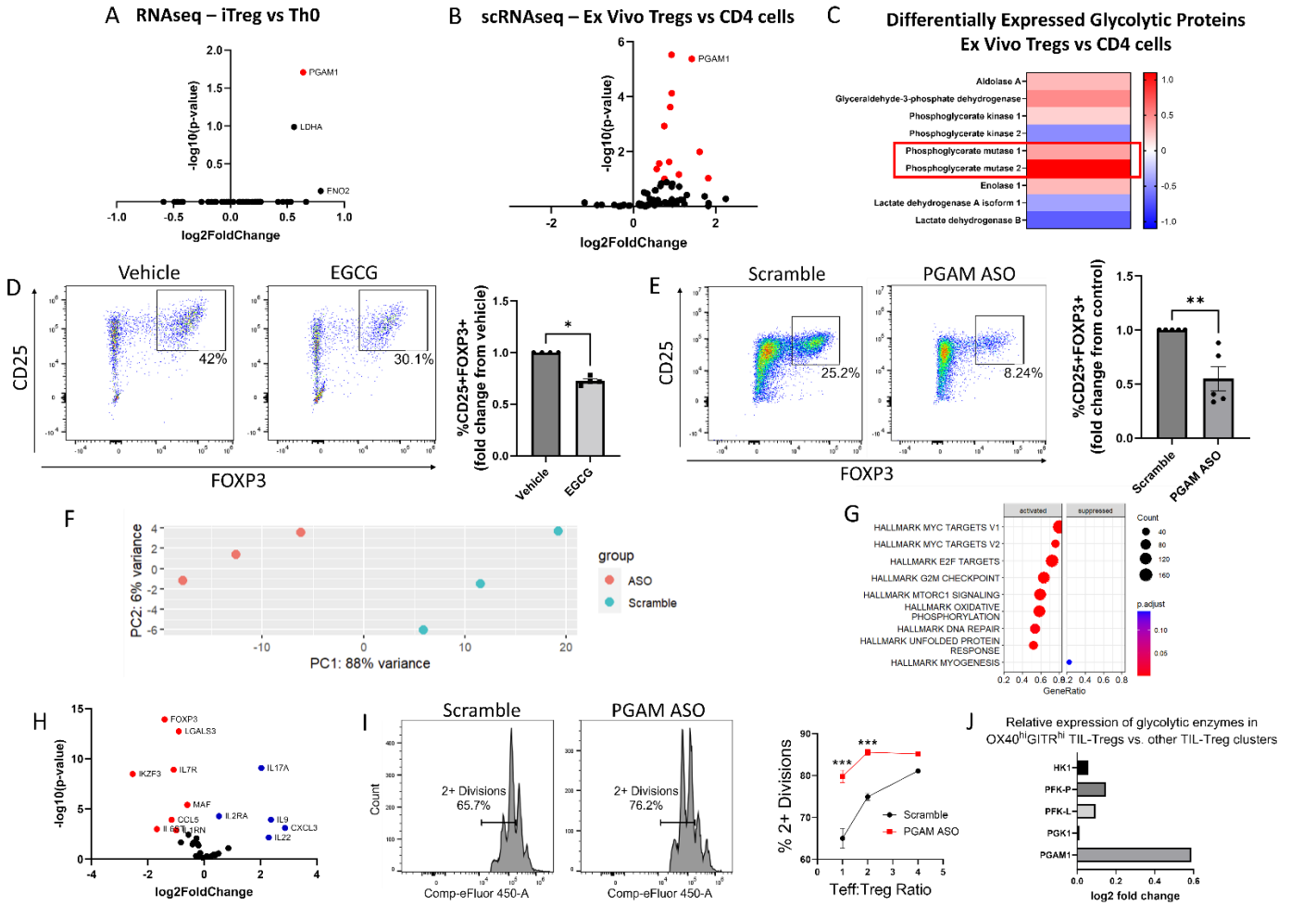

Figure 1. PGAM regulates Treg differentiation and suppressive function. (**A – C**) Analysis of publicly available transcriptomics and proteomics data reveals upregulation of PGAM expression in human iTregs and ex vivo Tregs. (**A**) Publicly available RNAseq data from human naïve CD4 cells cultured under either Th0 or Treg polarizing conditions for 72 hours (Ubaid Ullah et al., 2018) was analyzed, and genes belonging to the Gene Ontology (GO) term "Glycolysis and Gluconeogenesis" were plotted. (**B**) Differential expression of "Glycolysis and Gluconeogensis" GO genes in ex vivo Tregs vs. total CD4 cells derived from healthy donor PBMCs (Schafflick et al., 2020). *GAPDH* was removed for scaling purposes. (**C**) Differential expression of cytosolic glycolytic enzymes in ex vivo Tregs vs. conventional CD4 T cells derived from healthy donor PBMCs, analyzed from publicly available proteomics data (Procaccini et al., 2016). (**D**) Naïve murine CD4 cells were cultured under Treg polarizing conditions for 4 days and treated with either EGCG (20 μM) or vehicle on day 1. Treg polarization based on CD25 and FOXP3 expression was analyzed by flow cytometry. Data represent mean ± SEM from 4 independent experiments, with 3-4 biological replicates per experiment. (**E**) Naïve murine CD4 cells were treated with either scrambled or PGAM-specific antisense oligonucleotides (ASOs) and cultured under Treg polarizing conditions for 72 hours. CD25 and FOXP3 expression were analyzed by flow cytometry. Data represent mean ± SEM from 5 independent experiments, with 3-4 biological replicates per experiment. (**F – H**) Naïve murine CD4 cells were cultured with either scrambled or anti-PGAM ASOs for 72 hours under Treg polarizing conditions. RNA was isolated from unsorted cells for RNAseq, followed by library size normalization and differential expression analysis. Shown are (**F**) PCA plot for scrambled and anti-PGAM ASO-treated cells, (**G**) Gene Set Enrichment Analysis (GSEA) using MSigDB Hallmark gene sets and (**H**) volcano plot of genes associated with T cell function. Data from 3 biological replicates. (**I**) Naïve murine CD4 cells were cultured under Treg polarizing conditions with either scrambled or anti-PGAM ASOs for 72 hours. To assess Treg suppressive function, the polarized Tregs were cultured with naïve CD4 cells stimulated with CD3/CD28 stimulating antibodies for an additional 72 hours at the indicated ratios. Cell proliferation was measured by dilution of a cell proliferation dye. Data represent mean ± SEM from 4 biological replicates. (**J**) Analysis of a published scRNAseq dataset of tumor-infiltrating Tregs (TIL-Tregs) (Dykema et al., 2023) shows that *PGAM1* is overexpressed in the most highly suppressive subpopulation, out of proportion to proximal rate-limiting glycolytic enzymes. *$P < 0.05$, **$P < 0.01$, *** $P < 0.0001$ by Mann-Whitney U Test (D, E) or two-way ANOVA with multiple comparisons testing (I). P-values in (A), (B), and (F – H) were derived from Wald's test after False Discovery Rate correction and median-of-ratios normalization via DESeq2.

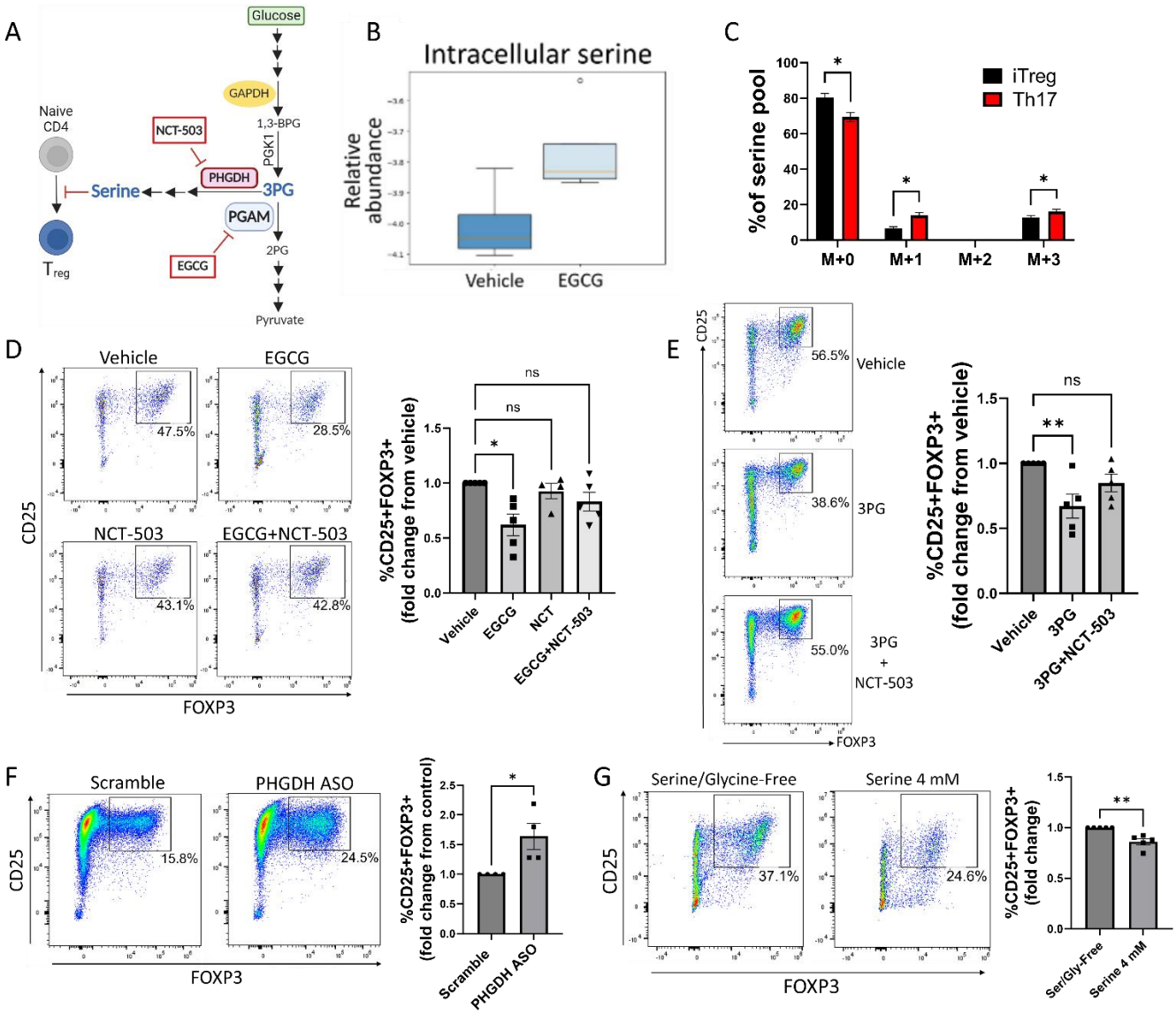

Figure 2. PGAM regulates Treg differentiation through control of de novo serine synthesis. (**A**) Schematic diagram of the intersection of glycolysis and the de novo serine synthesis pathway via the PGAM substrate 3PG. Pharmacologic inhibitors are shown in red boxes. (**B**) Naïve murine CD4 cells were cultured under Treg polarizing conditions for 4 days and treated with vehicle or EGCG (20 μM) on day 1. Unsorted cells were then lysed and metabolites were extracted and analyzed via LC-MS. Data from 4 biological replicates. (**C**) The rate of glucose-derived serine synthesis from polarized murine Tregs or Th17 cells was measured by adding $U^{13}C$-glucose to the culture media for 6 hours and quantifying the percentage of labeled/unlabeled serine via LC-MS. The mass isotopomer distribution (MID) of $U^{13}C$-glucose-derived serine and percent contribution to the total serine pool is shown. Data represent mean ± SEM from 3 biological replicates. (**D**) Naïve murine CD4 cells were cultured under Treg polarizing conditions for 4 days. On day 1, the cells were treated with vehicle or the indicated combinations of the PGAM inhibitor EGCG (10 μM) and the PHGDH inhibitor NCT-503 (10 μM) (doses optimized for combination treatment). Treg polarization was assayed by flow cytometry. Data represent mean ± SEM from 5 independent experiments. (**E**) Naïve murine CD4 cells were polarized under Treg conditions for 4 days. On day 1 of polarization, cells were either sham-electroporated or supplemented with 3PG (1.5 mM) by electroporation and treated with vehicle or the PHGDH inhibitor NCT-503 (10 μM). Analysis was performed by flow cytometry. Data represent mean ± SEM from 5 independent experiments. (**F**) Naïve CD4 cells were cultured under Treg polarizing conditions with either scrambled or anti-PHGDH ASOs, and Treg generation was analyzed by flow cytometry. Data represent mean ± SEM from 4 independent experiments. (**G**) Naïve murine CD4 cells were cultured under Treg polarizing conditions for 4 days with either serine/glycine-free media or serine/glycine-free media supplemented with 4 mM serine, followed by flow cytometric analysis. Data represent mean ± SEM from 5 independent experiments. *$P < 0.05$, **$P < 0.01$ by Mann-Whitney U test (F, G), Kruskal Wallis test with multiple comparisons testing (D, E), or student's t test with multiple hypothesis correction (C). Each independent experiment shown in D – G included 3-4 biological replicates.

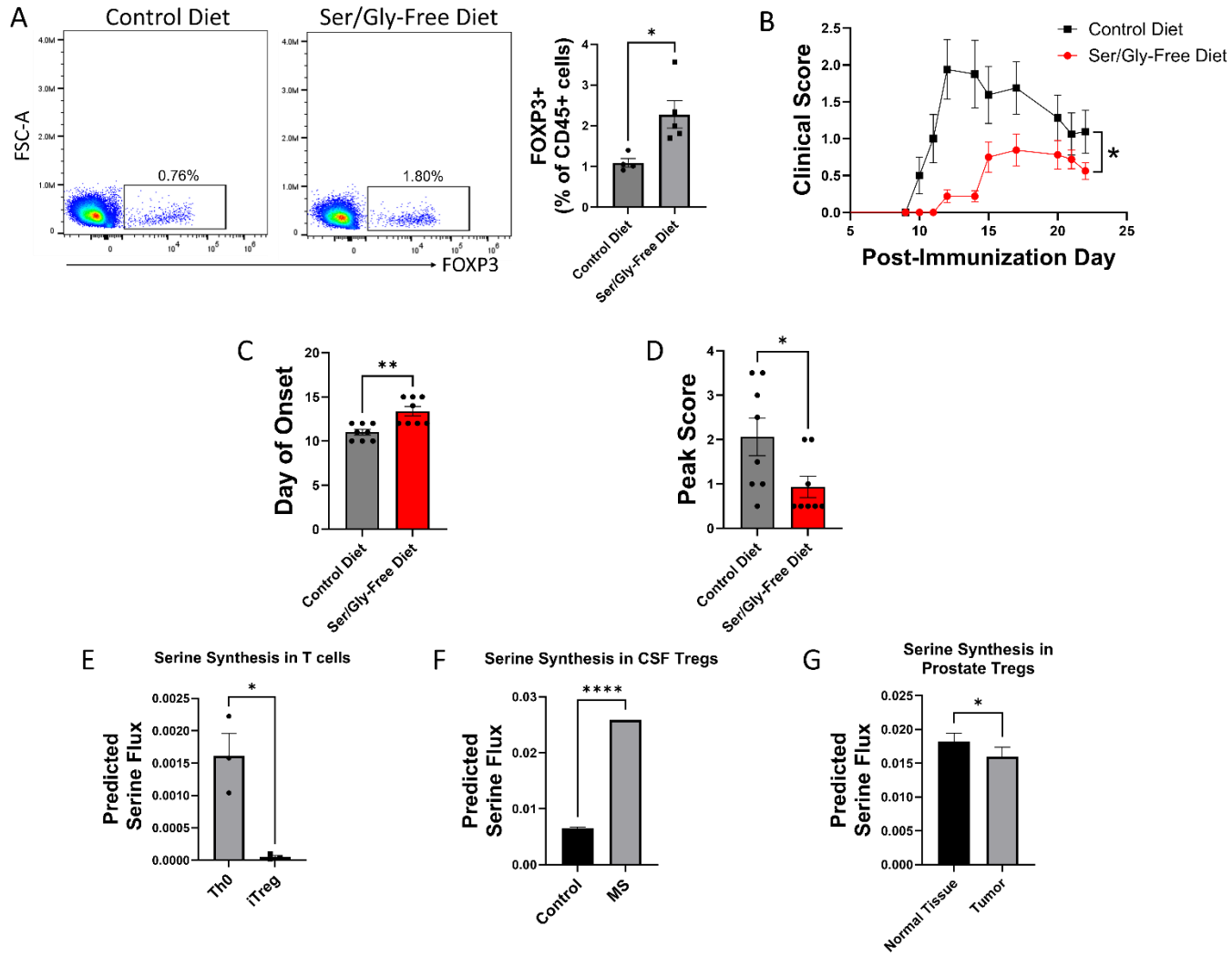

Figure 3. Serine synthesis and dietary availability regulate Tregs in vivo and in disease states. (**A**) C57BL/6 mice were fed either serine/glycine-free diet or control diet for 8 weeks, beginning immediately post-weaning. Peripheral Tregs from blood were quantified by flow cytometry as the percentage of $CD45^+$ cells expressing FOXP3. Data represent mean ± SEM from 4-5 mice per group. (**B – D**) Mice were fed either serine/glycine-free diet or control diet for 7 days and then subjected to MOG_{35-55} EAE. Clinical scoring was performed by a blinded observer. Data represent mean ± SEM from 8 mice per group. Shown are (**B**) clinical scores over the course of the experiment, (**C**) day of neurologic symptom onset, and (**D**) peak clinical scores. (**E – G**) Publicly available RNAseq data from three different datasets was analyzed using SCFEA to model serine synthesis rates from mRNA levels of metabolic enzymes. (**E**) SCFEA from human naïve CD4 cells cultured under either Th0 or Treg polarizing conditions for 72 hours (Ubaid Ullah et al., 2018) predicts decreased serine synthesis in iTregs. (**F**) Predicted serine synthesis is increased in Tregs derived from cerebrospinal fluid of patients with treatment-naïve relapsing MS compared to controls (Schafflick et al., 2020). (**G**) Predicted serine synthesis is decreased in Tregs derived from prostate cancer versus control prostate (Camps et al., 2023). *$P < 0.05$, **$P < 0.01$, **** $P<0.00001$ by student's t-test (A, E, F, G), Mann-Whitney U test (C, D), and two-way ANOVA with repeated measures (B).

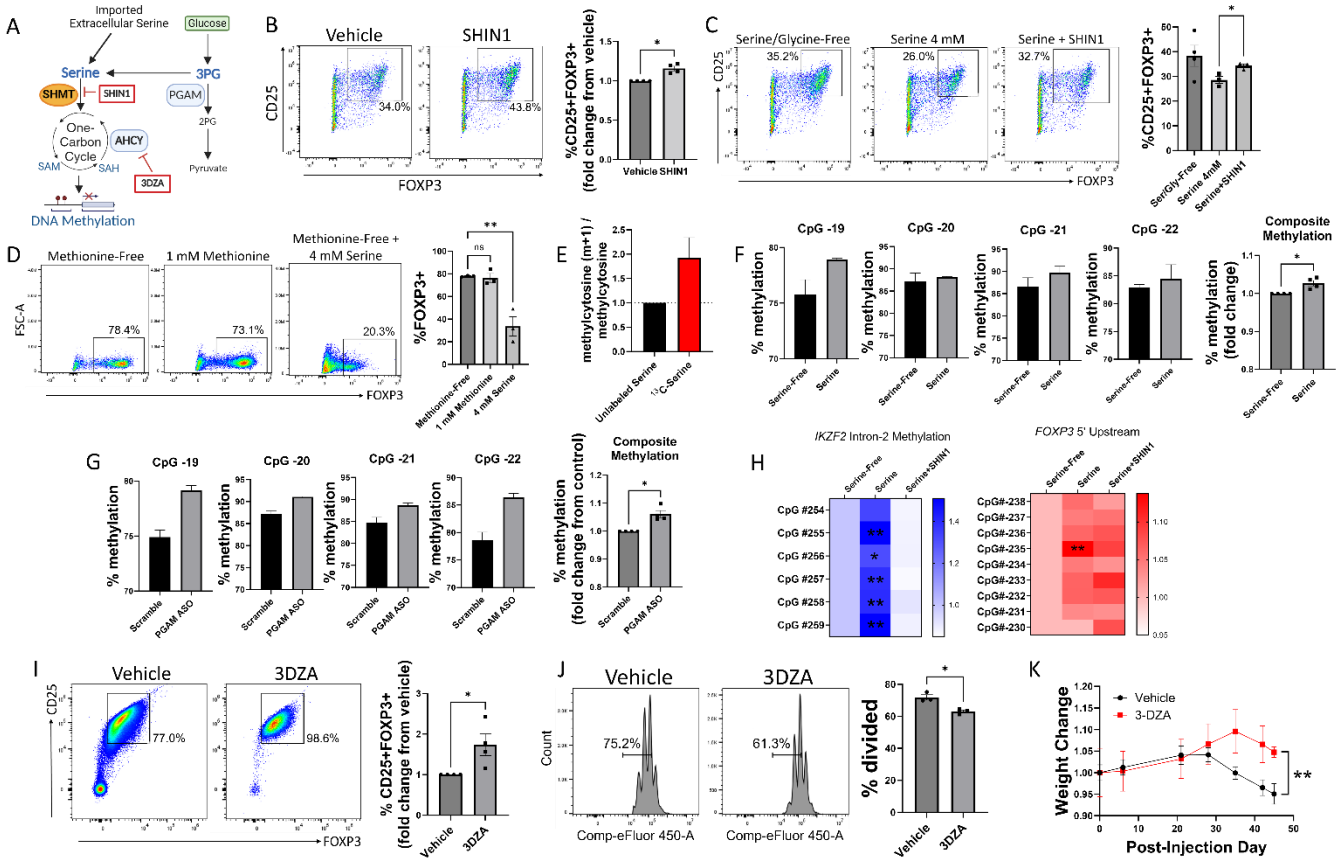

Figure 4. Serine inhibits Treg polarization by contributing to one-carbon metabolism and methylation of Treg-associated genes. (**A**) Schematic diagram of serine entry into one-carbon metabolism and the methyl donor cycle. Pharmacologic inhibitors are shown in red boxes. (**B**) Naïve murine CD4 cells were cultured under Treg polarizing conditions for 72 hours with either vehicle or SHIN1 (SHMT1/2 inhibitor, 1 μM) added at day 0 of culture. Treg polarization was assayed by flow cytometry. Data represent mean ± SEM from 4 independent experiments, with 3-4 biological replicates per experiment. (**C**) Naïve murine CD4 cells were cultured in serine/glycine-free media, media containing 4 mM serine, or media with serine plus SHIN1 (1 μM). Treg polarization was assayed by flow cytometry. Data represent mean ± SEM from 3-4 biological replicates per condition. (**D**) Naïve murine CD4 cells were cultured in methionine-free media supplemented with vehicle, 1 mM methionine, or 4 mM serine, and FOXP3 expression was assayed by flow cytometry. Data represent mean ± SEM from 3 biological replicates. (**E**) Naïve murine CD4 cells were cultured in serine/glycine-free media for 48 hours under Treg polarizing conditions and then for 12 hours with either unlabeled serine or $U^{13}C$-serine. The mass isotopomer ratio of carbon-labeled methylcytosine (m+1) / unlabeled methylcytosine from unsorted cells is shown. Data represent mean ± SEM from 3 biological replicates. (**F**) Naïve CD4 cells were cultured under Treg polarizing conditions with either serine/glycine-free media or 4 mM serine. Methylation at the FOXP3 TSDR was assayed by pyrosequencing from unsorted cells. The composite methylation was calculated as the percent methylation for each of the 4 CpG sites measured in the assay normalized to the serine/glycine-free condition. Data derived from 3 biological replicates per condition. (**G**) Naïve CD4 cells were cultured under Treg polarizing conditions with either scrambled or anti-PGAM ASOs. Methylation at the FOXP3 TSDR was assayed by pyrosequencing from unsorted cells. The composite methylation was calculated as the percent methylation at each of the 4 CpG sites measured in the assay normalized to scrambled control. Data derived from 3 biological replicates per condition. (**H**) Naïve murine CD4 cells were cultured in serine/glycine-free media, media containing 4 mM serine, or media with serine plus SHIN1 (1 μM). Bisulfite-treated DNA was sequenced from unsorted cells using a Treg-specific next generation sequencing panel, and percent methylation of key sites was calculated. Data derived from 3 biological replicates per condition. (**I**) Naïve CD4 cells were cultured under Treg polarizing conditions with either vehicle or 3-Deazaadenosine (3DZA, AHCY inhibitor, 5 μM). Treg polarization was assayed by flow cytometry. Data represent mean ± SEM from 4 independent experiments, with 3-4 biological replicates per experiment. (**J**) Naïve CD4 cells were polarized to Tregs with either vehicle or 3DZA and then cultured with CD4 cells stimulated with CD3/CD28 to evaluate Treg suppressive function. CD4 cell proliferation was measured by flow cytometry. Data represent mean ± SEM from 3 biological replicates. (**K**) Naïve CD4 cells were cultured under Treg polarizing conditions with either vehicle or 3DZA, and 10^6 cells were then transferred into RAG -/- mouse recipients along with 10^7 activated CD4 cells. Mice were weighed at the specified times and weights are shown relative to the weight at the day of injection. Data represent mean ± SEM from 5 mice per group. *$P < 0.05$, **$P < 0.01$ by Mann-Whitney U test (B, F, G, I), one-way ANOVA with Tukey's multiple comparisons testing (C, D), two-way ANOVA with Dunnett's multiple comparison testing (H), student's t-test of average final weight (K), or student's t test (J).

METHODS

Key resources table

REAGENT or RESOURCE	SOURCE	IDENTIFIER
Antibodies		
Anti-murine CD25, BV785	Biolegend	102051
Anti-murine FOXP3, APC	ThermoFisher	17-5773-80
Zombie NIR fixable viability	Biolegend	423106
PGAM1 Antibody [Alexa Fluor® 405]	Novus Biologicals	NBP1-49532AF405
CD3 Monoclonal Antibody (OKT3), Functional Grade, eBioscience™	Thermofisher	16-0037-81
CD28 Monoclonal Antibody (37.51), Functional Grade, eBioscience™	Thermofisher	16-0281-82
InVivoPlus anti-mouse IFNγ	BioXcell	BP0055
InVivoMAb anti-mouse IL-4	BioXcell	BE0045
Chemicals, peptides, and recombinant proteins		
SHIN1	MCE	HY-112066
NCT-503	Sigma	SML1659-5MG
EGCG	Millipore Sigma	E4143-50MG
3-DZA	Cayman	9000785
Heptelidic Acid	Cayman	14079
D-()-3-Phosphoglyceric Acid (Sodium Salt)	Cayman	20123
D-(+)-Glucose-13C6	Cayman	26707
L-Serine-13C3	Cayman	35126
Critical commercial assays		
Cell Proliferation Dye	eBioscience	65-0842-85
Deposited data		
RNA-sequencing data from scramble vs anti-PGAM ASO	This paper	GEO GSE269846
Experimental models: Organisms/strains		
C57BL/6J wild type mice	Jackson Laboratory	000664
B6.129S7-*Rag1*^{tm1Mom}/J (RAG knockout mice)	Jackson Laboratory	002216
Oligonucleotides		
Anti-sense PGAM1 oligonucleotides	Custom Order	Aum Biotech
Anti-sense PHGDH oligonucleotides	Custom Order	Aum Biotech
Other		
Animal-Free Recombinant Murine IL-2	AF-212-12	ThermoFisher
RECOMBINANT HUMAN TGF BETA 1	PHP143B	Biorad
Murine IL-6	216-16	Peprotech
Recombinant Mouse IL-23 (carrier-free)	589002	Biolegend
Murine IL-1beta	211-11B	Peprotech
MojoSort(TM) Mouse CD4 Naive T Cell Isolation Kit	480040	Biolegend
MojoSort(TM) Mouse CD4 T Cell Isolation Kit	480006	Biolegend
Serine/Glycine-free diet	1812281	Animal Specialty and Provisions

Control Diet	1817070-209	Animal Specialty and Provisions

Resource Availability

Lead Contact

Further information and requests for resources and reagents should be directed to and will be fulfilled by the Lead Contact, Michael D. Kornberg (michael.kornberg@jhmi.edu).

Materials Availability

This study did not generate new unique reagents.

Data and Code Availability

All data supporting the findings of this study are presented and/or tabulated within the Article or Supplemental Information. RNA-sequencing data from Figures 1F-1H has been deposited in the Gene Expression Omnibus (GEO) database and can be accessed via GEO accession number GSE269846.

Experimental Model and Subject Details

Animals

Wild type C57BL/6J (stock # 000664) and B6.129S7-*Rag1*^{tm1Mom}/J RAG knockout mice (stock # 002216) were purchased from The Jackson Laboratory. All mice were housed in a dedicated Johns Hopkins mouse facility. All protocols were approved by the Johns Hopkins Institutional Animal Care and Use Committee.

Primary Cell Cultures

CD4+ T-Cell Isolation and Culture

T-cells were isolated by generating single-cell suspensions from the spleen and lymph nodes of 6–10-week-old C57BL/6 mice. Spleens were mechanically dissociated with the plunger of a syringe over a 100-µm cell strainer (BD Falcon), then were pelleted by centrifugation (1500 RPM for 5 min) and resuspended in fresh FACS buffer. Naive CD4+ cells were isolated by negative selection using the MojoSort CD4+ naïve T-cell isolation kit from Biolegend (Catalog 480040) according to the manufacturer's instructions. Plates were coated overnight at 4°C with plate-bound anti-mouse CD3 antibody (2 µg/mL). Prior to plating, cells were resuspended in complete 50% RPMI (RPMI plus 10%FBS, 1% Pen-strep, 1% glutamax, 0.1% 2-mercaptoethanol) and 50 % AIM-V media along with 2 ug/mL soluble anti-mouse CD28 antibody. Experiments involving serine/glycine-free media or methionine-free media were done with 100% complete RPMI lacking the corresponding amino acid(s). Treg polarizing conditions included 10 ng/mL murine IL-2 and 1 ng/mL human TGF-β along with 5 ug/mL anti-mouse IFNγ and 5 ug/mL anti-mouse IL-4. Experiments with Treg polarization for Treg suppression assays were performed with 15 ng/mL human TGF-β and 10 ng/mL retinoic acid. Cells were not sorted prior to downstream assays, although bulk experiments were only performed on samples with greater than 70% cell viability (greater than 90% for stable isotope tracing studies).

Method Details

Drug and ASO Treatments

For drug treatments, cells were treated with the indicated drug at the indicated concentration. EGCG was dissolved in EtOH, while NCT-503 and SHIN1 were dissolved in DMSO. Vehicle controls for drug treatment experiments consisted of solvent alone. Antisense oligonucleotides (ASOs) were dissolved in PBS and added at 10 µM directly to the cell culture media starting at day 0. Control samples for ASO experiments were treated identically, but with scrambled ASOs.

Electroporation

For electroporation with 3-phosphoglycerate (3PG), naïve CD4 cells were cultured for 24 hours under Treg polarizing conditions, and pre-treated with NCT-503 or vehicle for 4 hours prior to electroporation as indicated. Cells were then harvested, centrifuged, and resuspended in BTX high performance electroporation solution (45-0803) with either 1.5 mM 3-PG or PBS as indicated. Electroporation was performed at 500 V for 3 ms with 1 pulse/square in a 4 mM BTX electroporation cuvette. Cells were then immediately added to complete RPMI media that contained 1.5 mM 3-PG or PBS and rested for 2-4 hours. Cells were then centrifuged and resuspended with the media they were in prior to electroporation.

Flow Cytometry

Cells were stained with zombie NIR (1:1000) for 10 minutes and then washed with Flow Wash Buffer (PBS+ 2% fetal bovine serum + 2 mM EDTA). They were then stained with anti-CD25 (BV785) for 30 minutes. Cells were then washed with Flow Wash buffer two times and fixed with FoxP3 fixation/permeabilization buffer following the manufacturer recommended protocol. Intracellular staining was performed with conjugated antibodies (1:200) against the specified proteins in permeabilization buffer for 1 h, washed twice, and then analyzed cells with a Cytek Aurora Flow cytometer. Data analysis was performed with FlowJo software.

Treg Suppression Assay

To generate Tregs for the Treg suppression assay, naïve CD4 T cells were cultured for 4 days under Treg polarizing conditions. Then, total CD4+ T cells were isolated from murine spleens using Biolegend Mojo CD4 T cell isolation kit (480006) and labelled with Cell Proliferation Dye (eBioscience, #65-0842-85) by incubating in a 1:2000 dilution (PBS) for 10 minutes, washing 1X with PBS, and then washing 2X with complete RPMI. CD4+ T cells were cultured as described above (3 ug/mL anti-CD3, 3 ug/mL anti-CD28, 10 ng/mL recombinant murine IL-2) with varying ratios of Treg:Teffector cells. Divisions were counted by measuring cell proliferation dye dilutions with flow cytometry after a 3-day culture.

Mouse Peripheral Blood Samples

Mice were fed either serine/glycine-free diet or control diet (Animal Specialty and Provisions, 1812281 and 1817070-209) for 8 weeks immediately post-weaning and peripheral blood samples were obtained via cheek bleed into a microfuge tube coated with heparin/EDTA. RBCs were lysed with RBC lysis buffer for 7 minutes and then the reaction was stopped with HBSS (including Calcium and Magnesium). Cells were then stained with zombie NIR (1:1000) and anti-CD16/32 (1:200) for 10 minutes then stained with anti-CD45, anti-CD11b and anti-CD4 for 30 minutes. Staining then proceeded as described in the flow cytometry section.

Mass Spectrometry

Sample preparation for steady-state measurement of serine involved culturing CD4 T cells for 72 hours under Treg polarizing conditions, followed by treatment with the indicated drugs for 24 hours. The cells were collected, washed with PBS, and equal numbers of cells per condition were pelleted and flash-frozen. The frozen cell pellets were shipped to the Metabolomics Core at Baylor College of Medicine, Houston, TX. The cells were then resuspended in a 500-µl mixture of 1:1 water/methanol, sonicated for one minute (two 30-second pulses), and mixed with 450 µl of ice-cold chloroform. The resulting homogenate was combined with 150 µl of ice-cold water, vortexed for five minutes, incubated at –20°C for 30 minutes, and centrifuged at 4°C for ten minutes to partition the aqueous and organic layers. The combined layers were dried at 37°C for 45 minutes in a SpeedVac system (Genevac EZ Solvent Evaporator, SP Industries, Inc.). The extract was reconstituted in a 500-µl solution of methanol/water (1:1) and filtered through a 3-kDa molecular filter (Amicon® Ultra Centrifugal Filter, 3 kDa MWCO, Millipore Sigma) at 4°C for 90 minutes to remove proteins. The filtrate was dried at 37°C for 90 minutes in a SpeedVac and stored at –80°C until mass spectrometric analysis. Prior to mass spectrometric analysis, the dried extract was resuspended in methanol/water (1:1).

For amino acid flux analysis, CD4 T cells were cultured for 6 hours in glucose-free media, then 12 mM U13C-glucose was added for 6 hours. The cells were resuspended in a 500-µl mixture of 1:1 water/methanol, sonicated for one minute (two 30-second pulses), centrifuged at 4°C for ten minutes, and filtered through a 3-kDa molecular filter (Amicon® Ultra Centrifugal Filter, 3 kDa MWCO, Millipore Sigma) at 4°C for 90 minutes to remove proteins. The samples were dried at 37°C for 45 minutes in a SpeedVac system (Genevac EZ Solvent Evaporator, SP Industries, Inc.). Prior to mass spectrometry analysis, the dried extract was resuspended in methanol/water (1:1).

CD4 T cells were cultured under Treg polarizing conditions in serine-free media to measure methylcytosine flux, followed by the addition of either normal serine or 13C3-serine for 12 hours. The cells were harvested, the pellets were washed, and DNA was isolated using the Qiagen DNeasy Blood & Tissue Kit. DNA was quantified with a Nanodrop, and all samples were normalized based on total DNA content before mass spectrometry analysis. The details of the DNA hydrolysis methods were previously described (PMID: 27158554). DNA was denatured at 100°C for 3 minutes, incubated with ammonium acetate and nuclease P1, then mixed and incubated with venom phosphodiesterase I, followed by incubation with alkaline phosphatase. The details of the liquid chromatography-mass spectrometry (LC-MS) methods were also described earlier (PMID: 27158554).

For the LC-MS analysis method for serine steady state and tracing study of serine and methylcytosine, chromatographic separation of extracted metabolites, including serine, was performed through Hydrophilic Interaction Chromatography (HILIC) using an XBridge Amide column (3.5 µm, 4.6 x 100 mm, Waters, Milford, MA) in ESI-positive ionization mode. Solvent A (0.1% formic acid in water) and Solvent B (0.1% formic acid in acetonitrile) were used for chromatographic separation (Ref). The data were acquired via multiple reaction monitoring (MRM) using a 6495 Triple Quadrupole mass spectrometer coupled to an HPLC system (Agilent Technologies, Santa Clara, CA) through Agilent Mass Hunter Data Acquisition Software (ver. 10.1) (PMID: 31360899, PMID: 30642841). The acquired mass spectra were analyzed and integrated into each targeted compound peak using Agilent Mass Hunter Quantitative Analysis Software. For serine measurement, peak areas were normalized with a spiked internal standard. Differential metabolites were determined using p-values from t-tests following the Benjamini-Hochberg method, with a false discovery rate (FDR) of less than 0.25. For serine and methylcytosine tracing studies, the percentage of 13C incorporation was calculated using Microsoft Excel from peak areas and represented as bar graphs.

EAE Induction and Scoring

Active EAE was induced in female and male C57BL/6J mice[76–78] (10 weeks old) after pretreatment with either serine/glycine-free diet or control diet (Animal Specialty and Provisions, 1812281 and 1817070-209) for one week. MOG_{35-55} peptide dissolved in PBS at a concentration of 2 mg/mL was mixed 1:1 with complete Freund's adjuvant (8 mg/ml Tuberculin toxin in incomplete Freund's adjuvant), then mixed for 12 min into an emulsion. On day 0, mice were immunized by injecting 75 µl of the emulsion subcutaneously into each of two sites on the lateral abdomen. In addition, on day 0 and again on day 2, mice were injected intraperitoneally with 375 ng pertussis toxin. Scoring was performed by a blinded individual according to the following scale: 0, no clinical deficit; 0.5, partial loss of tail tone; 1.0, complete tail paralysis or both partial loss of tail tone plus awkward gait; 1.5, complete tail paralysis and awkward gait; 2.0, tail paralysis with hind limb weakness evidenced by foot dropping between bars of cage lid while walking; 2.5, hind limb paralysis with little to no weight-bearing on hind limbs (dragging), but with some movement possible in legs; 3.0, complete hind limb paralysis with no movement in lower limbs; 3.5, hind limb paralysis with some weakness in forelimbs; 4.0, complete tetraplegia but with some movement of head; 4.5, moribund; and 5.0, dead.

RNA-Seq

For all experiments, RNA was isolated using the Qiagen RNeasy Mini Plus Kit. For RNA-seq, library preparation, sequencing, and demultiplexing was performed by Novogene. Raw FASTQ files were aligned to the murine reference genome with Kallisto [79]. Library size normalization and differential expression was performed with DESeq2 [80,81]. Pathway enrichment analysis was performed with GSEA [82,83], and hypergeometric tests were performed with EnrichR [84].

Single Cell Flux Estimation Analysis (SCFEA)

Re-analysis of publicly available data was performed by downloading the relevant dataset from the GEO repository or from figshare. Gene count matrices were extracted and then analyzed with the SCFEA python package or web server. The rate of de novo serine synthesis was estimated with the reaction titled "3PG -> Serine." Comparisons between groups was performed with either student's t-test or Wilcox Rank sum test as described in the figure legends.

Bisulfite Conversion and Pyrosequencing

Bisulfite conversion was performed by EpigenDx according to standard pyrosequencing and Next Gen Sequencing protocols. Briefly, cell pellets were lysed based on the total cell count per sample and total volume received using M-digestion Buffer (ZymoResearch; Irvine, CA; cat# D5021-9) and 5-10µL of protease K (20mg/mL), with a final M-digestion concentration of 1X. The samples were incubated at 65°C for a minimum of 2 hours. For bisulfite modification, 20µL of the supernatant from the sample extracts was bisulfite modified using the EZ-96 DNA Methylation-Direct Kit™ (ZymoResearch; Irvine, CA; cat# D5023) as per the manufacturer's protocol. The bisulfite modified DNA samples were eluted using Melution buffer in 46µL. For Multiplex PCR, all bisulfite modified DNA samples were amplified using separate multiplex or simplex PCRs. PCRs included 0.5 units of HotStarTaq (Qiagen; Hilden, Germany; cat# 203205), 0.2µM primers, and 3µL of bisulfite-treated DNA in a 20µL reaction. All PCR products were verified using the Qiagen QIAxcel Advanced System (v1.0.6). Prior to library preparation, PCR products from the same sample were pooled and then purified using the QIAquick PCR Purification Kit columns or plates (cat# 28106 or 28183). The PCR cycling conditions were: 95°C 15 min; 45 x (95°C 30s; Ta°C 30 s; 68°C 30 s); 68°C 5 min; 4°C ∞. Samples were run alongside established reference DNA samples with a range of methylation. They were created by mixing high- and low-methylated DNA to obtain samples with 0, 50, and 100% methylation. The high-methylated DNA was *in vitro* enzymatically methylated genomic DNA with >85% methylation. The low-methylated DNA was chemically and enzymatically treated with <5% methylation. They were first tested on numerous gene-specific and global methylation assays using pyrosequencing.

Methylation Sequencing

Libraries were prepared using a custom Library Preparation method created by EpigenDx. Next, library molecules were purified using Agencourt AMPure XP beads (Beckman Coulter; Brea, CA; cat# A63882). Barcoded samples were then pooled in an equimolar fashion before template preparation and enrichment were performed on the Ion Chef™ system using Ion 520™ & Ion 530™ ExT Chef reagents (Thermo Fisher; Waltham, MA; cat# A30670). Following this, enriched, template-positive library molecules were sequenced on the Ion S5™ sequencer using an Ion 530™ sequencing chip (cat# A27764). FASTQ files from the Ion Torrent S5 server were aligned to a local reference database using the open-source Bismark Bisulfite Read Mapper program (v0.12.2) with the Bowtie2 alignment algorithm (v2.2.3). Methylation levels were calculated in Bismark by dividing the number of methylated reads by the total number of reads. An R-squared value (RSQ) was previously calculated from controls set at known methylation levels to test for PCR bias.

T-cell Transfer Model of Inflammatory Bowel Disease

To induce autoimmune colitis, CD4 T cells were transferred into RAG-knockout mice (Jackson Laboratories #002216). Briefly, CD4 cells were isolated from wild-type C57BL/6 mice and cultured in a mixture of 50% cRPMI (RPMI+10% Fetal Bovine Serum, 1 % penicillin-streptomycin, and 0.1% 2-Mercaptoethanol) and 50% AIM-V media with plate bound anti-CD3 stimulation (3 ug/mL) and anti-CD28 stimulation (2 ug/mL) along with 10 ng/mL murine IL-2. Cells were stimulated for 3 days, rested for 2 days, and then re-stimulated for 2 days. 10 million activated cells were then transferred into each mouse via i.p. injection. At the same time, naïve CD4 cells were cultured under Treg polarizing conditions as described above and 1 million cells were transferred into each mouse at the same time as the injection of the activated cells. Weights were recorded weekly until euthanasia.

Quantification and Statistical Analysis

All statistical analyses were performed using GraphPad Prism software, Python, or R studio. Details of statistical analyses for each experiment and/or data set can be found in the figures and figure legends. When cumulative data was tabulated from multiple independent experiments, experimental groups from each independent experiment were normalized to a matched control condition to allow integration across experiments. In these cases, in which there is no variability among matched control values, statistical analysis was performed with a non-parametric test as outlined in standard statistical guidelines (doi: 10.1111/bph.14153).

REFERENCES

1. Patel, C.H., and Powell, J.D. (2017). Targeting T cell metabolism to regulate T cell activation, differentiation and function in disease. Curr Opin Immunol *46*, 82–88. https://doi.org/10.1016/J.COI.2017.04.006.

2. Buck, M. (2016). Mitochondrial dynamics controls T cell fate through metabolic programming. Cell *166*, 63–76.

3. Chapman, N.M., and Chi, H. (2022). Metabolic adaptation of lymphocytes in immunity and disease. Immunity *55*, 14–30. https://doi.org/10.1016/J.IMMUNI.2021.12.012.

4. Geltink, R.I.K., Kyle, R.L., and Pearce, E.L. (2018). Unraveling the Complex Interplay between T Cell Metabolism and Function. Annu Rev Immunol *36*, 461–488. https://doi.org/10.1146/annurev-immunol-042617-053019.

5. Kelly, B., and O'Neill, L.A.J. (2015). Metabolic reprogramming in macrophages and dendritic cells in innate immunity. Cell Research 2015 25:7 *25*, 771–784. https://doi.org/10.1038/cr.2015.68.

6. Kornberg, M.D. (2020). The immunologic Warburg effect: Evidence and therapeutic opportunities in autoimmunity. Wiley Interdiscip Rev Syst Biol Med *12*, e1486. https://doi.org/10.1002/WSBM.1486.

7. O'Neill, L.A.J., Kishton, R.J., and Rathmell, J. (2016). A guide to immunometabolism for immunologists. Nature Reviews Immunology 2016 16:9 *16*, 553–565. https://doi.org/10.1038/nri.2016.70.

8. Frauwirth, K.A., Riley, J.L., Harris, M.H., Parry, R. V., Rathmell, J.C., Plas, D.R., Elstrom, R.L., June, C.H., and Thompson, C.B. (2002). The CD28 signaling pathway regulates glucose metabolism. Immunity *16*, 769–777. https://doi.org/10.1016/S1074-7613(02)00323-0.

9. Cham, C.M., and Gajewski, T.F. (2005). Glucose Availability Regulates IFN-γ Production and p70S6 Kinase Activation in CD8+ Effector T Cells. The Journal of Immunology *174*, 4670–4677. https://doi.org/10.4049/JIMMUNOL.174.8.4670.

10. Cham, C.M., Driessens, G., O'Keefe, J.P., and Gajewski, T.F. (2008). Glucose deprivation inhibits multiple key gene expression events and effector functions in CD8+ T cells. Eur J Immunol *38*, 2438–2450. https://doi.org/10.1002/EJI.200838289.

11. Wang, R., Dillon, C.P., Shi, L.Z., Milasta, S., Carter, R., Finkelstein, D., McCormick, L.L., Fitzgerald, P., Chi, H., Munger, J., et al. (2011). The Transcription Factor Myc Controls Metabolic Reprogramming upon T Lymphocyte Activation. Immunity *35*, 871–882. https://doi.org/10.1016/J.IMMUNI.2011.09.021.

12. Chang, C.-H. (2013). Posttranscriptional control of T cell effector function by aerobic glycolysis. Cell *153*, 1239–1251.

13. Macintyre, A.N., Gerriets, V.A., Nichols, A.G., Michalek, R.D., Rudolph, M.C., Deoliveira, D., Anderson, S.M., Abel, E.D., Chen, B.J., Hale, L.P., et al. (2014). The Glucose Transporter Glut1 Is Selectively Essential for CD4 T Cell Activation and Effector Function. Cell Metab *20*, 61–72. https://doi.org/10.1016/J.CMET.2014.05.004.

14. Gerriets, V.A., Kishton, R.J., Nichols, A.G., MacIntyre, A.N., Inoue, M., Ilkayeva, O., Winter, P.S., Liu, X., Priyadharshini, B., Slawinska, M.E., et al. (2015). Metabolic programming and PDHK1 control CD4+ T cell subsets and inflammation. Journal of Clinical Investigation *125*, 194–207. https://doi.org/10.1172/JCI76012.

15. Shi, L.Z., Wang, R., Huang, G., Vogel, P., Neale, G., Green, D.R., and Chi, H. (2011). HIF1α-dependent glycolytic pathway orchestrates a metabolic checkpoint for the differentiation of TH17 and Treg cells. Journal of Experimental Medicine *208*, 1367–1376. https://doi.org/10.1084/jem.20110278.

16. Shi, H., and Chi, H. (2019). Metabolic Control of Treg Cell Stability, Plasticity, and Tissue-Specific Heterogeneity. Front Immunol *10*, 491785. https://doi.org/10.3389/FIMMU.2019.02716/BIBTEX.

17. Angelin, A., Gil-de-Gómez, L., Dahiya, S., Jiao, J., Guo, L., Levine, M.H., Wang, Z., Quinn, W.J., Kopinski, P.K., Wang, L., et al. (2017). Foxp3 Reprograms T Cell Metabolism to Function in Low-Glucose, High-Lactate Environments. Cell Metab *25*, 1282-1293.e7. https://doi.org/10.1016/j.cmet.2016.12.018.

18. Ho, P.C., Bihuniak, J.D., MacIntyre, A.N., Staron, M., Liu, X., Amezquita, R., Tsui, Y.C., Cui, G., Micevic, G., Perales, J.C., et al. (2015). Phosphoenolpyruvate Is a Metabolic Checkpoint of Anti-tumor T Cell Responses. Cell *162*, 1217–1228. https://doi.org/10.1016/j.cell.2015.08.012.

19. Wang, H., Franco, F., Tsui, Y.C., Xie, X., Trefny, M.P., Zappasodi, R., Mohmood, S.R., Fernández-García, J., Tsai, C.H., Schulze, I., et al. (2020). CD36-mediated metabolic adaptation supports regulatory T cell survival and function in tumors. Nature Immunology 2020 21:3 *21*, 298–308. https://doi.org/10.1038/s41590-019-0589-5.

20. Lim, S.A., Wei, J., Nguyen, T.L.M., Shi, H., Su, W., Palacios, G., Dhungana, Y., Chapman, N.M., Long, L., Saravia, J., et al. (2021). Lipid signalling enforces functional specialization of Treg cells in tumours. Nature 2021 591:7849 *591*, 306–311. https://doi.org/10.1038/s41586-021-03235-6.

21. Kishore, M., Cheung, K.C.P., Fu, H., Bonacina, F., Wang, G., Coe, D., Ward, E.J., Colamatteo, A., Jangani, M., Baragetti, A., et al. (2017). Regulatory T Cell Migration Is Dependent on Glucokinase-Mediated Glycolysis. Immunity *47*, 875-889.e10. https://doi.org/10.1016/j.immuni.2017.10.017.

22. Angelin, A., Gil-de-Gómez, L., Dahiya, S., Jiao, J., Guo, L., Levine, M.H., Wang, Z., Quinn, W.J., Kopinski, P.K., Wang, L., et al. (2017). Foxp3 Reprograms T Cell Metabolism to Function in Low-Glucose, High-Lactate Environments. Cell Metab *25*, 1282-1293.e7. https://doi.org/10.1016/J.CMET.2016.12.018.

23. Michalek, R.D., Gerriets, V.A., Jacobs, S.R., Macintyre, A.N., MacIver, N.J., Mason, E.F., Sullivan, S.A., Nichols, A.G., and Rathmell, J.C. (2011). Cutting Edge: Distinct Glycolytic and Lipid Oxidative Metabolic Programs Are Essential for Effector and Regulatory CD4+ T Cell Subsets. The Journal of Immunology *186*, 3299–3303. https://doi.org/10.4049/JIMMUNOL.1003613.

24. Gerriets, V.A., Kishton, R.J., Johnson, M.O., Cohen, S., Siska, P.J., Nichols, A.G., Warmoes, M.O., De Cubas, A.A., MacIver, N.J., Locasale, J.W., et al. (2016). Foxp3 and Toll-like receptor signaling balance Treg cell anabolic metabolism for suppression. Nature Immunology 2016 17:12 *17*, 1459–1466. https://doi.org/10.1038/ni.3577.

25. Macintyre, A.N., Gerriets, V.A., Nichols, A.G., Michalek, R.D., Rudolph, M.C., Deoliveira, D., Anderson, S.M., Abel, E.D., Chen, B.J., Hale, L.P., et al. (2014). The Glucose Transporter Glut1 Is Selectively Essential for CD4 T Cell Activation and Effector Function. Cell Metab *20*, 61–72. https://doi.org/10.1016/J.CMET.2014.05.004.

26. Wei, J., Long, L., Yang, K., Guy, C., Shrestha, S., Chen, Z., Wu, C., Vogel, P., Neale, G., Green, D.R., et al. (2016). Autophagy enforces functional integrity of regulatory T cells by coupling environmental cues and metabolic homeostasis. Nature Immunology 2016 17:3 *17*, 277–285. https://doi.org/10.1038/ni.3365.

27. Scherlinger, M., Pan, W., Hisada, R., Boulougoura, A., Yoshida, N., Vukelic, M., Umeda, M., Krishfield, S., Tsokos, M.G., and Tsokos, G.C. (2022). Phosphofructokinase P fine-tunes T regulatory cell metabolism, function, and stability in systemic autoimmunity. Sci Adv *8*, 9657. https://doi.org/10.1126/SCIADV.ADC9657/SUPPL_FILE/SCIADV.ADC9657_DATA_FILES_S1_TO_S4.ZIP.

28. Kornberg, M.D., Bhargava, P., Kim, P.M., Putluri, V., Snowman, A.M., Putluri, N., Calabresi, P.A., and Snyder, S.H. (2018). Dimethyl fumarate targets GAPDH and aerobic glycolysis to modulate immunity. Science (1979) *360*, 449–453. https://doi.org/10.1126/science.aan4665.

29. Gerriets, V.A., Kishton, R.J., Nichols, A.G., MacIntyre, A.N., Inoue, M., Ilkayeva, O., Winter, P.S., Liu, X., Priyadharshini, B., Slawinska, M.E., et al. (2015). Metabolic programming and PDHK1 control CD4+ T cell subsets and inflammation. J Clin Invest *125*, 194–207. https://doi.org/10.1172/JCI76012.

30. De Rosa, V., Galgani, M., Porcellini, A., Colamatteo, A., Santopaolo, M., Zuchegna, C., Romano, A., De Simone, S., Procaccini, C., La Rocca, C., et al. (2015). Glycolysis controls the induction of human regulatory T cells by modulating the expression of FOXP3 exon 2 splicing variants. Nature Immunology 2015 16:11 *16*, 1174–1184. https://doi.org/10.1038/ni.3269.

31. Ubaid Ullah, Andrabi, S.B.A., Tripathi, S.K., Dirasantha, O., Kanduri, K., Rautio, S., Gross, C.C., Lehtimäki, S., Bala, K., Tuomisto, J., et al. (2018). Transcriptional Repressor HIC1 Contributes to Suppressive Function of Human Induced Regulatory T Cells. Cell Rep *22*, 2094–2106. https://doi.org/10.1016/J.CELREP.2018.01.070.

32. Schafflick, D., Xu, C.A., Hartlehnert, M., Cole, M., Schulte-Mecklenbeck, A., Lautwein, T., Wolbert, J., Heming, M., Meuth, S.G., Kuhlmann, T., et al. (2020). Integrated single cell analysis of blood and cerebrospinal fluid leukocytes in multiple sclerosis. Nature Communications 2020 11:1 *11*, 1–14. https://doi.org/10.1038/s41467-019-14118-w.

33. Procaccini, C., Carbone, F., Di Silvestre, D., Brambilla, F., De Rosa, V., Galgani, M., Faicchia, D., Marone, G., Tramontano, D., Corona, M., et al. (2016). The Proteomic Landscape of Human Ex Vivo Regulatory and Conventional T Cells Reveals Specific Metabolic Requirements. Immunity *44*, 406–421. https://doi.org/10.1016/J.IMMUNI.2016.01.028.

34. Li, X., Tang, S., Wang, Q.Q., Leung, E.L.H., Jin, H., Huang, Y., Liu, J., Geng, M., Huang, M., Yuan, S., et al. (2017). Identification of Epigallocatechin-3- Gallate as an Inhibitor of Phosphoglycerate Mutase 1. Front Pharmacol *8*, 325. https://doi.org/10.3389/FPHAR.2017.00325.

35. Dykema, A.G., Zhang, J., Cheung, L.S., Connor, S., Zhang, B., Zeng, Z., Cherry, C.M., Li, T., Caushi, J.X., Nishimoto, M., et al. (2023). Lung tumor–infiltrating Treg have divergent transcriptional profiles and function linked to checkpoint blockade response. Sci Immunol *8*. https://doi.org/10.1126/SCIIMMUNOL.ADG1487/SUPPL_FILE/SCIIMMUNOL.ADG1487_MDAR_REPRODUCIBILITY_CHECKLIST.PDF.

36. Brenes, A.J., Lamond, A.I., and Cantrell, D.A. (2023). The Immunological Proteome Resource. Nature Immunology 2023, 1–1. https://doi.org/10.1038/s41590-023-01483-4.

37. Dimauro, S., Miranda, A.F., Khan, S., Gitlin, K., and Friedman, R. (1981). Human Muscle Phosphoglycerate Mutase Deficiency: Newly Discovered Metabolic Myopathy. Science (1979) *212*, 1277–1279. https://doi.org/10.1126/SCIENCE.6262916.

38. Koo, B., and Oskarsson, B. (2016). Phosphoglycerate mutase deficiency (glycogen storage disease X) caused by a novel variant in PGAM-M. Neuromuscular Disorders *26*, 688–690. https://doi.org/10.1016/J.NMD.2016.08.002.

39. Lunt, S.Y., and Vander Heiden, M.G. (2011). Aerobic Glycolysis: Meeting the Metabolic Requirements of Cell Proliferation. https://doi.org/10.1146/annurev-cellbio-092910-154237 *27*, 441–464. https://doi.org/10.1146/ANNUREV-CELLBIO-092910-154237.

40. He, L., Ding, Y., Zhou, X., Li, T., and Yin, Y. (2023). Serine signaling governs metabolic homeostasis and health. Trends in Endocrinology and Metabolism *34*, 361–372. https://doi.org/10.1016/j.tem.2023.03.001.

41. Ron-Harel, N., Santos, D., Ghergurovich, J.M., Sage, P.T., Reddy, A., Lovitch, S.B., Dephoure, N., Satterstrom, F.K., Sheffer, M., Spinelli, J.B., et al. (2016). Mitochondrial Biogenesis and Proteome Remodeling Promote One-Carbon Metabolism for T Cell Activation. Cell Metab *24*, 104–117. https://doi.org/10.1016/j.cmet.2016.06.007.

42. Ma, E.H., Bantug, G., Griss, T., Condotta, S., Johnson, R.M., Samborska, B., Mainolfi, N., Suri, V., Guak, H., Balmer, M.L., et al. (2017). Serine Is an Essential Metabolite for Effector T Cell Expansion. Cell Metab *25*, 345–357. https://doi.org/10.1016/j.cmet.2016.12.011.

43. Kurniawan, H., Franchina, D.G., Guerra, L., Bonetti, L., Baguet, L.S., Grusdat, M., Schlicker, L., Hunewald, O., Dostert, C., Merz, M.P., et al. (2020). Glutathione Restricts Serine Metabolism to Preserve Regulatory T Cell Function. Cell Metab *31*, 920-936.e7. https://doi.org/10.1016/j.cmet.2020.03.004.

44. Bojkova, D., Reus, P., Panosch, L., Bechtel, M., Rothenburger, T., Kandler, J.D., Pfeiffer, A., Wagner, J.U.G., Shumliakivska, M., Dimmeler, S., et al. (2023). Identification of novel antiviral drug candidates using an optimized SARS-CoV-2 phenotypic screening platform. iScience *26*, 105944. https://doi.org/10.1016/J.ISCI.2023.105944.

45. Pacold, M.E., Brimacombe, K.R., Chan, S.H., Rohde, J.M., Lewis, C.A., Swier, L.J.Y.M., Possemato, R., Chen, W.W., Sullivan, L.B., Fiske, B.P., et al. (2016). A PHGDH inhibitor reveals coordination of serine synthesis and one-carbon unit fate. Nature Chemical Biology 2016 12:6 *12*, 452–458. https://doi.org/10.1038/nchembio.2070.

46. Alghamdi, N., Chang, W., Dang, P., Lu, X., Wan, C., Gampala, S., Huang, Z., Wang, J., Ma, Q., Zang, Y., et al. (2021). A graph neural network model to estimate cell-wise metabolic flux using single-cell RNA-seq data. Genome Res *31*, 1867–1884. https://doi.org/10.1101/GR.271205.120/-/DC1.

47. Tuong, Z.K., Loudon, K.W., Berry, B., Richoz, N., Jones, J., Tan, X., Nguyen, Q., George, A., Hori, S., Field, S., et al. (2021). Resolving the immune landscape of human prostate at a single-cell level in health and cancer. Cell Rep *37*. https://doi.org/10.1016/J.CELREP.2021.110132.

48. Camps, J., Noël, F., Liechti, R., Massenet-Regad, L., Rigade, S., Götz, L., Hoffmann, C., Amblard, E., Saichi, M., Ibrahim, M.M., et al. (2023). Meta-Analysis of Human Cancer Single-Cell RNA-Seq Datasets Using the IMMUcan Database. Cancer Res *83*, 363–373. https://doi.org/10.1158/0008-5472.CAN-22-0074/711421/AM/META-ANALYSIS-OF-HUMAN-CANCER-SINGLE-CELL-RNA-SEQ.

49. Reina-Campos, M., Diaz-Meco, M.T., and Moscat, J. (2020). The complexity of the serine glycine one-carbon pathway in cancer. Journal of Cell Biology *219*. https://doi.org/10.1083/JCB.201907022/132493.

50. Makino, Y., Oe, C., Iwama, K., Suzuki, S., Nishiyama, A., Hasegawa, K., Okuda, H., Hirata, K., Ueno, M., Kawaji, K., et al. (2022). Serine hydroxymethyltransferase as a potential target of antibacterial agents acting synergistically with one-carbon metabolism-related inhibitors. Communications Biology 2022 5:1 *5*, 1–12. https://doi.org/10.1038/s42003-022-03555-x.

51. Ducker, G.S., Ghergurovich, J.M., Mainolfi, N., Suri, V., Jeong, S.K., Li, S.H.J., Friedman, A., Manfredi, M.G., Gitai, Z., Kim, H., et al. (2017). Human SHMT inhibitors reveal defective glycine import as a targetable metabolic vulnerability of diffuse large B-cell lymphoma. Proc Natl Acad Sci U S A *114*, 11404–11409. https://doi.org/10.1073/PNAS.1706617114/SUPPL_FILE/PNAS.1706617114.ST02.DOCX.

52. Maddocks, O.D.K., Labuschagne, C.F., Adams, P.D., and Vousden, K.H. (2016). Serine Metabolism Supports the Methionine Cycle and DNA/RNA Methylation through De Novo ATP Synthesis in Cancer Cells. Mol Cell *61*, 210–221. https://doi.org/10.1016/J.MOLCEL.2015.12.014.

53. Mentch, S.J., and Locasale, J.W. (2016). One-carbon metabolism and epigenetics: understanding the specificity. Ann N Y Acad Sci *1363*, 91–98. https://doi.org/10.1111/NYAS.12956.

54. Polansky, J.K., Kretschmer, K., Freyer, J., Floess, S., Garbe, A., Baron, U., Olek, S., Hamann, A., von Boehmer, H., and Huehn, J. (2008). DNA methylation controls Foxp3 gene expression. Eur J Immunol *38*, 1654–1663. https://doi.org/10.1002/EJI.200838105.

55. Jeong, S.Y., Ahn, S.G., Lee, J.H., Kim, H.S., Kim, J.W., Rhim, H., Jeong, S.W., and Kim, I.K. (1999). 3-Deazaadenosine, a S-adenosylhomocysteine hydrolase inhibitor, has dual effects on NF-κB regulation: Inhibition of NF-κB transcriptional activity and promotion of IκBα degradation. Journal of Biological Chemistry *274*, 18981–18988. https://doi.org/10.1074/jbc.274.27.18981.

56. Michalek, R.D., Gerriets, V.A., Jacobs, S.R., Macintyre, A.N., MacIver, N.J., Mason, E.F., Sullivan, S.A., Nichols, A.G., and Rathmell, J.C. (2011). Cutting Edge: Distinct Glycolytic and Lipid Oxidative Metabolic Programs Are Essential for Effector and Regulatory CD4+ T Cell Subsets. The Journal of Immunology *186*, 3299–3303. https://doi.org/10.4049/JIMMUNOL.1003613.

57. Macintyre, A.N., Gerriets, V.A., Nichols, A.G., Michalek, R.D., Rudolph, M.C., Deoliveira, D., Anderson, S.M., Abel, E.D., Chen, B.J., Hale, L.P., et al. (2014). The glucose transporter Glut1 is selectively essential for CD4 T cell activation and effector function. Cell Metab *20*, 61–72. https://doi.org/10.1016/j.cmet.2014.05.004.

58. Shi, L.Z., Wang, R., Huang, G., Vogel, P., Neale, G., Green, D.R., and Chi, H. (2011). HIF1α–dependent glycolytic pathway orchestrates a metabolic checkpoint for the differentiation of TH17 and Treg cells. Journal of Experimental Medicine *208*, 1367–1376. https://doi.org/10.1084/JEM.20110278.

59. Lee, J., Walsh, M.C., Hoehn, K.L., James, D.E., Wherry, E.J., and Choi, Y. (2014). Regulator of Fatty Acid Metabolism, Acetyl Coenzyme A Carboxylase 1, Controls T Cell Immunity. The Journal of Immunology *192*, 3190–3199. https://doi.org/10.4049/jimmunol.1302985.

60. Berod, L., Friedrich, C., Nandan, A., Freitag, J., Hagemann, S., Harmrolfs, K., Sandouk, A., Hesse, C., Castro, C.N., BäHre, H., et al. (2014). De novo fatty acid synthesis controls the fate between regulatory T and T helper 17 cells. Nat Med *20*. https://doi.org/10.1038/nm.3704.

61. Tanimine, N., Germana, S.K., Fan, M., Hippen, K., Blazar, B.R., Markmann, J.F., Turka, L.A., and Priyadharshini, B. (2019). Differential effects of 2-deoxy-D-glucose on in vitro expanded human regulatory T cell subsets. PLoS One *14*, e0217761. https://doi.org/10.1371/JOURNAL.PONE.0217761.

62. Patel, C.H., Leone, R.D., Horton, M.R., and Powell, J.D. (2019). Targeting metabolism to regulate immune responses in autoimmunity and cancer. Nature Reviews Drug Discovery 2019 18:9 *18*, 669–688. https://doi.org/10.1038/s41573-019-0032-5.

63. McPhedran, S.J., Carleton, G.A., and Lum, J.J. (2024). Metabolic engineering for optimized CAR-T cell therapy. Nature Metabolism 2024 6:3 *6*, 396–408. https://doi.org/10.1038/s42255-024-00976-2.

64. Nanjireddy, P.M., Olejniczak, S.H., and Buxbaum, N.P. (2023). Targeting of chimeric antigen receptor T cell metabolism to improve therapeutic outcomes. Front Immunol *14*, 1121565. https://doi.org/10.3389/FIMMU.2023.1121565/BIBTEX.

65. Chan, J.D., Scheffler, C.M., Munoz, I., Sek, K., Lee, J.N., Huang, Y.-K., Yap, K.M., Saw, N.Y.L., Li, J., Chen, A.X.Y., et al. (2024). FOXO1 enhances CAR T cell stemness, metabolic fitness and efficacy. Nature 2024, 1–10. https://doi.org/10.1038/s41586-024-07242-1.

66. Good, Z., Spiegel, J.Y., Sahaf, B., Malipatlolla, M.B., Ehlinger, Z.J., Kurra, S., Desai, M.H., Reynolds, W.D., Wong Lin, A., Vandris, P., et al. (2022). Post-infusion CAR TReg cells identify patients resistant to CD19-CAR therapy. Nature Medicine 2022 28:9 *28*, 1860–1871. https://doi.org/10.1038/s41591-022-01960-7.

67. Zhang, Q., Lu, W., Liang, C.L., Chen, Y., Liu, H., Qiu, F., and Dai, Z. (2018). Chimeric antigen receptor (CAR) Treg: A promising approach to inducing immunological tolerance. Front Immunol *9*, 385915. https://doi.org/10.3389/FIMMU.2018.02359/BIBTEX.

68. Abraham, A.R., Maghsoudlou, P., Copland, D.A., Nicholson, L.B., and Dick, A.D. (2023). CAR-Treg cell therapies and their future potential in treating ocular autoimmune conditions. Frontiers in Ophthalmology *3*, 1184937. https://doi.org/10.3389/FOPHT.2023.1184937.

69. Toriyama, K., Kuwahara, M., Kondoh, H., Mikawa, T., Takemori, N., Konishi, A., Yorozuya, T., Yamada, T., Soga, T., Shiraishi, A., et al. (2020). T cell-specific deletion of Pgam1 reveals a critical role for glycolysis in T cell responses. Communications Biology 2020 3:1 *3*, 1–13. https://doi.org/10.1038/s42003-020-01122-w.

70. Itoyama, R., Yasuda-Yoshihara, N., Kitamura, F., Yasuda, T., Bu, L., Yonemura, A., Uchihara, T., Arima, K., Hu, X., Jun, Z., et al. (2021). Metabolic shift to serine biosynthesis through 3-PG accumulation and PHGDH induction promotes tumor growth in pancreatic cancer. Cancer Lett *523*, 29–42. https://doi.org/10.1016/J.CANLET.2021.09.007.

71. Zafari, P., Yari, K., Mostafaei, S., Iranshahi, N., Assar, S., Fekri, A., and Taghadosi, M. (2018). Analysis of Helios gene expression and Foxp3 TSDR methylation in the newly diagnosed Rheumatoid Arthritis patients. Immunol Invest *47*, 632–642. https://doi.org/10.1080/08820139.2018.1480029.

72. Toker, A., Engelbert, D., Garg, G., Polansky, J.K., Floess, S., Miyao, T., Baron, U., Düber, S., Geffers, R., Giehr, P., et al. (2013). Active Demethylation of the Foxp3 Locus Leads to the Generation of Stable Regulatory T Cells within the Thymus. The Journal of Immunology *190*, 3180–3188. https://doi.org/10.4049/JIMMUNOL.1203473.

73. Polansky, J.K., Kretschmer, K., Freyer, J., Floess, S., Garbe, A., Baron, U., Olek, S., Hamann, A., von Boehmer, H., and Huehn, J. (2008). DNA methylation controls Foxp3 gene expression. Eur J Immunol *38*, 1654–1663. https://doi.org/10.1002/EJI.200838105.

74. Kressler, C., Gasparoni, G., Nordström, K., Hamo, D., Salhab, A., Dimitropoulos, C., Tierling, S., Reinke, P., Volk, H.D., Walter, J., et al. (2021). Targeted De-Methylation of the FOXP3-TSDR Is Sufficient to Induce Physiological FOXP3 Expression but Not a Functional Treg Phenotype. Front Immunol *11*, 609891. https://doi.org/10.3389/FIMMU.2020.609891/BIBTEX.

75. Sugiura, A., Andrejeva, G., Voss, K., Heintzman, D.R., Xu, X., Madden, M.Z., Ye, X., Beier, K.L., Chowdhury, N.U., Wolf, M.M., et al. (2022). MTHFD2 is a metabolic checkpoint controlling effector and regulatory T cell fate and function. Immunity *55*, 65-81.e9. https://doi.org/10.1016/J.IMMUNI.2021.10.011.

76. Abramson, E., Hardman, C., Shimizu, A.J., Hwang, S., Hester, L.D., Snyder, S.H., Wender, P.A., Kim, P.M., and Kornberg, M.D. (2021). Designed PKC-targeting bryostatin analogs modulate innate immunity and neuroinflammation. Cell Chem Biol *0*. https://doi.org/10.1016/j.chembiol.2020.12.015.

77. Gharibani, P., Abramson, E., Shanmukha, S., Smith, M.D., Godfrey, W.H., Lee, J.J., Hu, J., Baydyuk, M., Dorion, M.-F., Deng, X., et al. (2025). The protein kinase C modulator bryostatin-1 therapeutically targets microglia to attenuate neuroinflammation and promote remyelination. ScienceTranslational Medicine *17*, eadk3434.

78. Godfrey, W.H., Hwang, S., Gharibani, P., Abramson, E., and Kornberg, M.D. (2023). Therapeutic Potential of Blocking GAPDH Nitrosylation with CGP3466b in Experimental Autoimmune Encephalomyelitis. Frontiers in Neuro. https://doi.org/10.1101/2022.08.31.505712.

79. Bray, N.L., Pimentel, H., Melsted, P., and Pachter, L. (2016). Near-optimal probabilistic RNA-seq quantification. Nature Biotechnology 2016 34:5 *34*, 525–527. https://doi.org/10.1038/nbt.3519.

80. Love, M.I., Huber, W., and Anders, S. (2014). Moderated estimation of fold change and dispersion for RNA-seq data with DESeq2. Genome Biol *15*, 1–21. https://doi.org/10.1186/S13059-014-0550-8/FIGURES/9.

81. Muzellec, B., Teleńczuk, M., Cabeli, V., and Andreux, M. (2023). PyDESeq2: a python package for bulk RNA-seq differential expression analysis. Bioinformatics *39*. https://doi.org/10.1093/BIOINFORMATICS/BTAD547.

82. Reimand, J., Isserlin, R., Voisin, V., Kucera, M., Tannus-Lopes, C., Rostamianfar, A., Wadi, L., Meyer, M., Wong, J., Xu, C., et al. (2019). Pathway enrichment analysis and visualization of omics data using g:Profiler, GSEA, Cytoscape and EnrichmentMap. Nature Protocols 2019 14:2 *14*, 482–517. https://doi.org/10.1038/s41596-018-0103-9.

83. Fang, Z., Liu, X., and Peltz, G. (2023). GSEApy: a comprehensive package for performing gene set enrichment analysis in Python. Bioinformatics *39*. https://doi.org/10.1093/BIOINFORMATICS/BTAC757.

84. Kuleshov, M. V., Jones, M.R., Rouillard, A.D., Fernandez, N.F., Duan, Q., Wang, Z., Koplev, S., Jenkins, S.L., Jagodnik, K.M., Lachmann, A., et al. (2016). Enrichr: a comprehensive gene set enrichment analysis web server 2016 update. Nucleic Acids Res *44*, W90. https://doi.org/10.1093/NAR/GKW377.

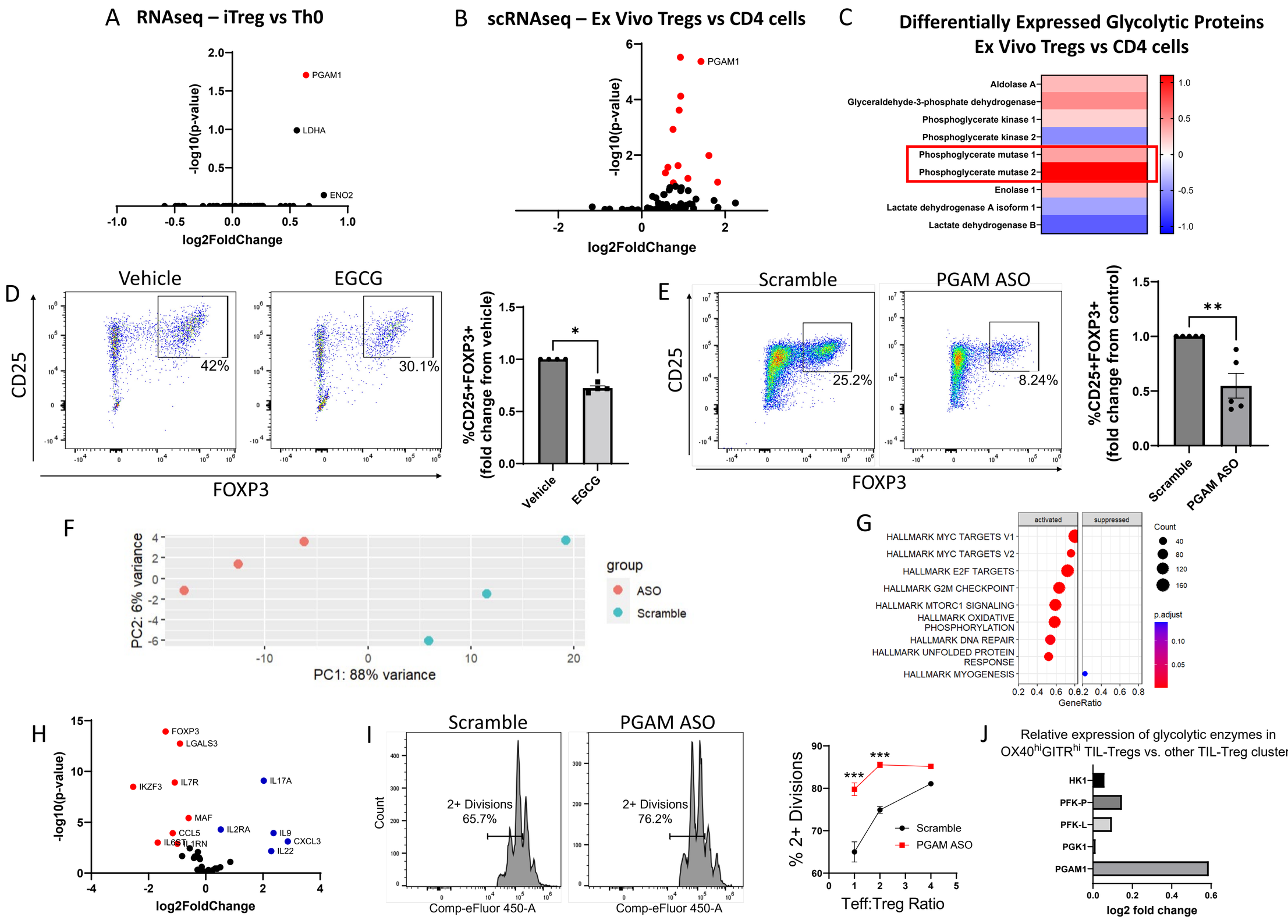
A
RNAseq – iTreg vs Th0
PGAM1
LDHA
ENO2
-log10(p-value)
log2FoldChange
B
scRNAseq – Ex Vivo Tregs vs CD4 cells
PGAM1
-log10(p-value)
log2FoldChange
C
Differentially Expressed Glycolytic Proteins
Ex Vivo Tregs vs CD4 cells
Aldolase A
Glyceraldehyde-3-phosphate dehydrogenase
Phosphoglycerate kinase 1
Phosphoglycerate kinase 2
Phosphoglycerate mutase 1
Phosphoglycerate mutase 2
Enolase 1
Lactate dehydrogenase A isoform 1
Lactate dehydrogenase B
D
Vehicle
EGCG
CD25
FOXP3
42%
30.1%
%CD25+FOXP3+ (fold change from vehicle)
Vehicle
EGCG
E
Scramble
PGAM ASO
CD25
FOXP3
25.2%
8.24%
%CD25+FOXP3+ (fold change from control)
Scramble
PGAM ASO
F
PC2: 6% variance
PC1: 88% variance
group
ASO
Scramble
G
activated
suppressed
HALLMARK MYC TARGETS V1
HALLMARK MYC TARGETS V2
HALLMARK E2F TARGETS
HALLMARK G2M CHECKPOINT
HALLMARK MTORC1 SIGNALING
HALLMARK OXIDATIVE PHOSPHORYLATION
HALLMARK DNA REPAIR
HALLMARK UNFOLDED PROTEIN RESPONSE
HALLMARK MYOGENESIS
GeneRatio
Count
p.adjust
H
FOXP3
LGALS3
IKZF3
IL7R
IL17A
MAF
IL2RA
CCL5
IL6ST
IL1RN
IL9
CXCL3
IL22
-log10(p-value)
log2FoldChange
I
Scramble
PGAM ASO
2+ Divisions 65.7%
2+ Divisions 76.2%
Count
Comp-eFluor 450-A
% 2+ Divisions
Teff:Treg Ratio
Scramble
PGAM ASO
J
Relative expression of glycolytic enzymes in OX40hiGITRhi TIL-Tregs vs. other TIL-Treg clusters
HK1
PFK-P
PFK-L
PGK1
PGAM1
log2 fold change

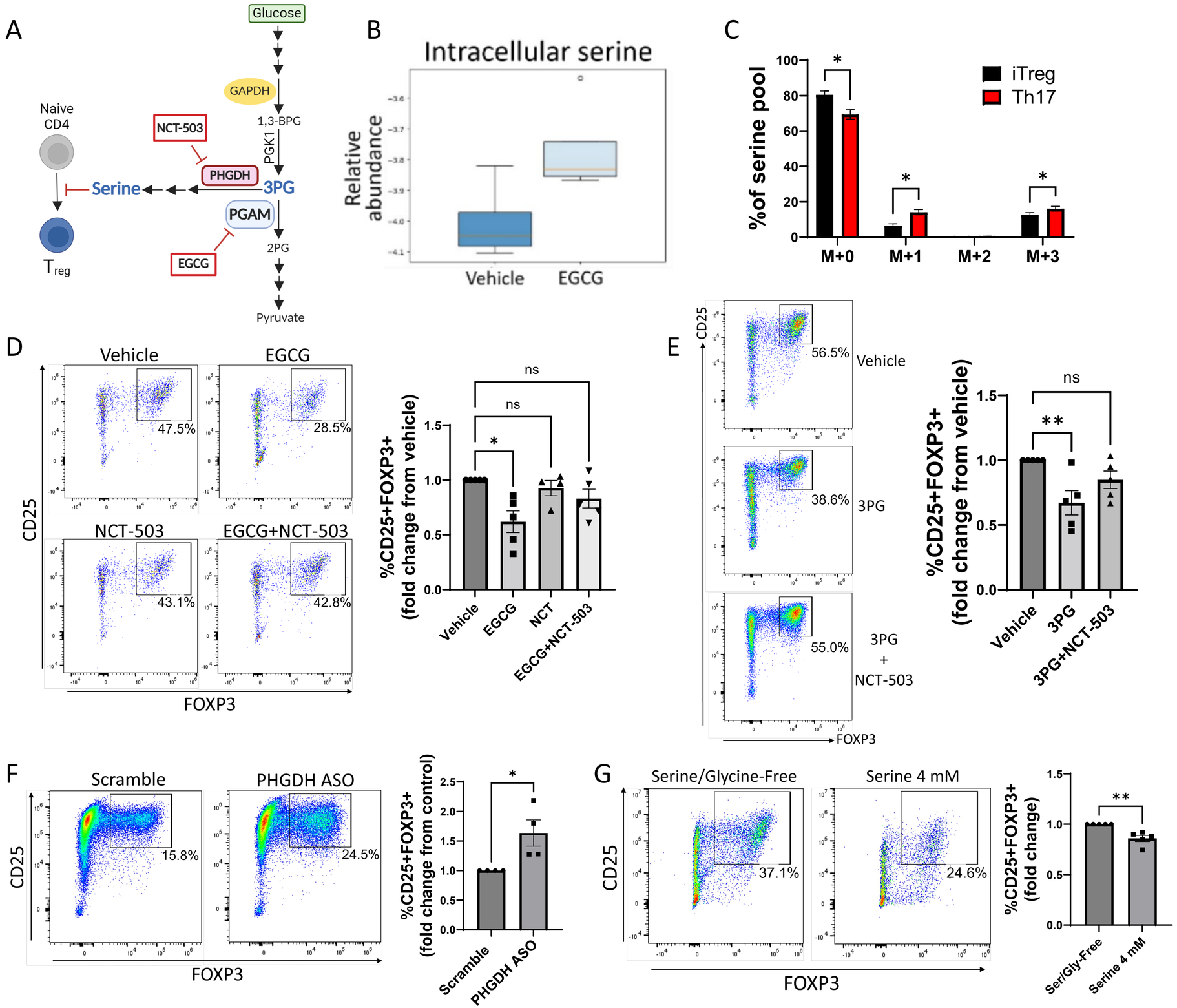
A
Glucose
GAPDH
1,3-BPG
PGK1
NCT-503
PHGDH
3PG
Serine
PGAM
2PG
EGCG
Pyruvate
Naive CD4
Treg
B
Intracellular serine
Relative abundance
Vehicle
EGCG
C
%of serine pool
iTreg
Th17
M+0
M+1
M+2
M+3
D
Vehicle
EGCG
NCT-503
EGCG+NCT-503
47.5%
28.5%
43.1%
42.8%
CD25
FOXP3
%CD25+FOXP3+ (fold change from vehicle)
ns
ns
*
Vehicle
EGCG
NCT
EGCG+NCT-503
E
CD25
56.5%
Vehicle
38.6%
3PG
55.0%
3PG + NCT-503
FOXP3
%CD25+FOXP3+ (fold change from vehicle)
ns
**
Vehicle
3PG
3PG+NCT-503
F
Scramble
PHGDH ASO
15.8%
24.5%
CD25
FOXP3
%CD25+FOXP3+ (fold change from control)
*
Scramble
PHGDH ASO
G
Serine/Glycine-Free
Serine 4 mM
37.1%
24.6%
CD25
FOXP3
%CD25+FOXP3+ (fold change)
**
Ser/Gly-Free
Serine 4 mM

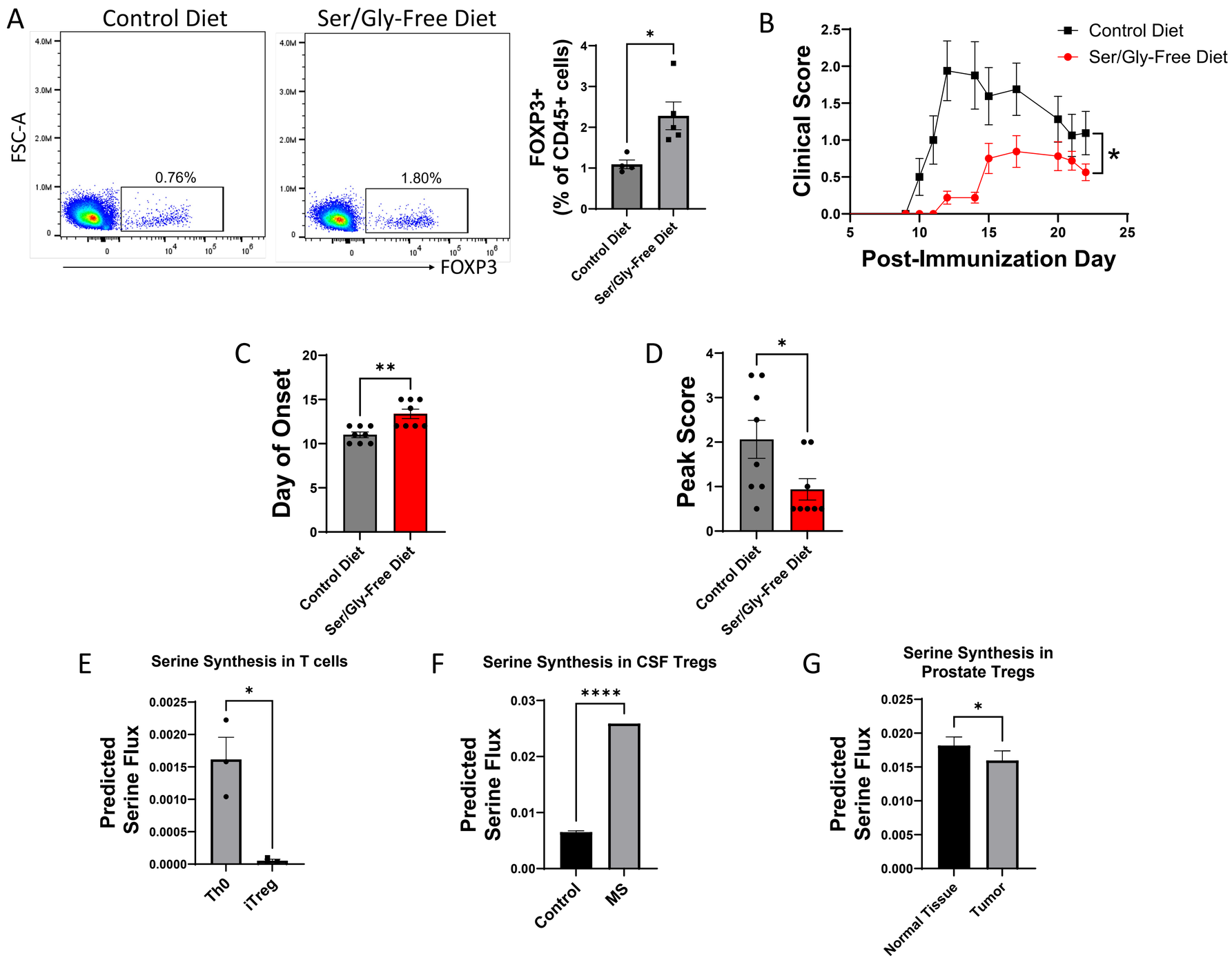
A
Control Diet
Ser/Gly-Free Diet
FSC-A
0.76%
1.80%
FOXP3
FOXP3+ (% of CD45+ cells)
Control Diet
Ser/Gly-Free Diet
B
Control Diet
Ser/Gly-Free Diet
Clinical Score
Post-Immunization Day
C
Day of Onset
Control Diet
Ser/Gly-Free Diet
D
Peak Score
Control Diet
Ser/Gly-Free Diet
E
Serine Synthesis in T cells
Predicted Serine Flux
Th0
iTreg
F
Serine Synthesis in CSF Tregs
Predicted Serine Flux
Control
MS
G
Serine Synthesis in Prostate Tregs
Predicted Serine Flux
Normal Tissue
Tumor

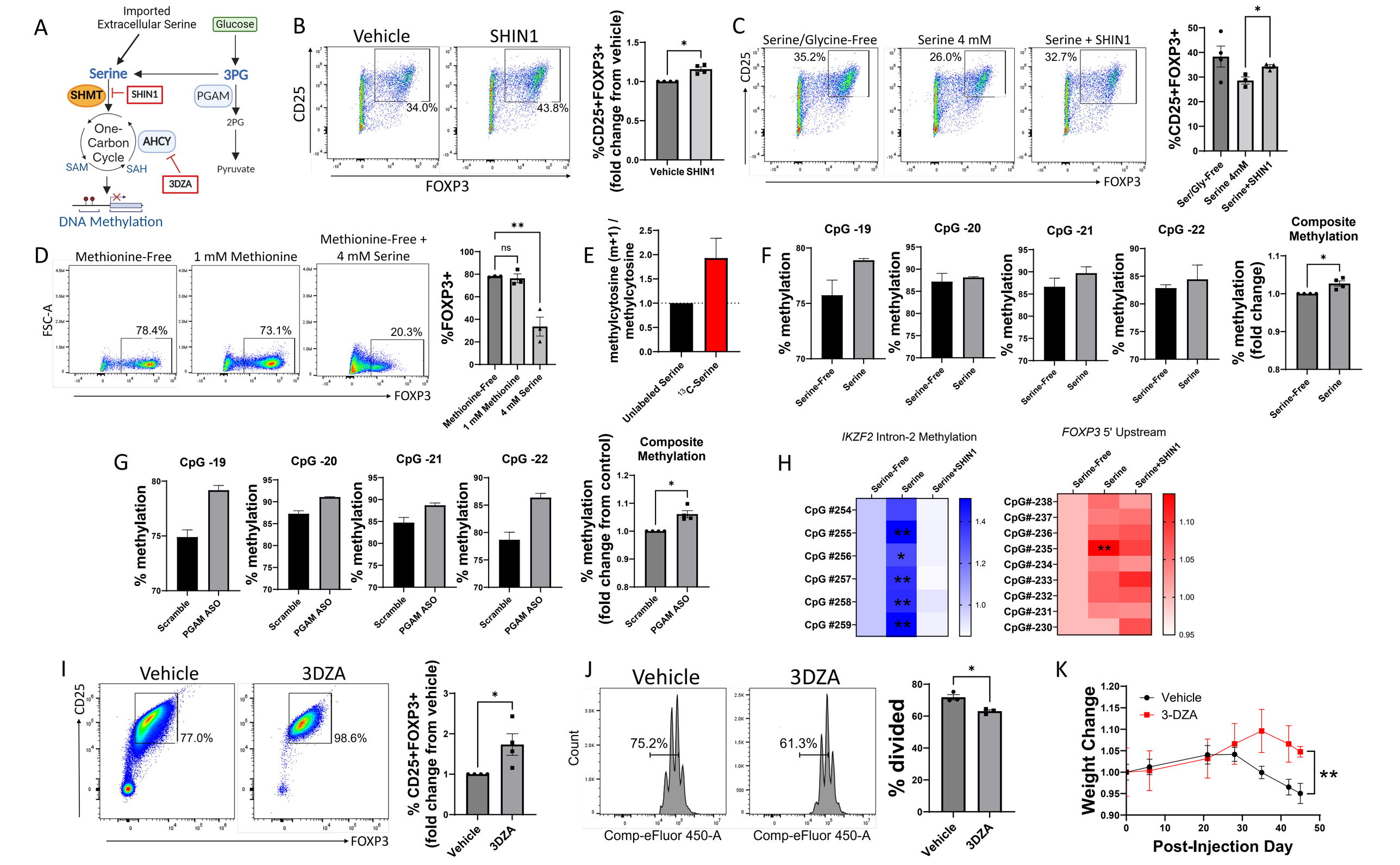
A
Imported Extracellular Serine
Glucose
Serine
3PG
SHMT
SHIN1
PGAM
2PG
One-Carbon Cycle
AHCY
SAM
SAH
3DZA
Pyruvate
DNA Methylation
B
Vehicle
SHIN1
CD25
FOXP3
34.0%
43.8%
%CD25+FOXP3+ (fold change from vehicle)
Vehicle SHIN1
C
Serine/Glycine-Free
Serine 4 mM
Serine + SHIN1
35.2%
26.0%
32.7%
%CD25+FOXP3+
Ser/Gly-Free
Serine 4mM
Serine+SHIN1
D
Methionine-Free
1 mM Methionine
Methionine-Free + 4 mM Serine
FSC-A
78.4%
73.1%
20.3%
%FOXP3+
ns
Methionine-Free
1 mM Methionine
4 mM Serine
E
methylcytosine (m+1) / methylcytosine
Unlabeled Serine
13C-Serine
F
CpG -19
CpG -20
CpG -21
CpG -22
Composite Methylation
% methylation
% methylation (fold change)
Serine-Free
Serine
G
CpG -19
CpG -20
CpG -21
CpG -22
Composite Methylation
% methylation
% methylation (fold change from control)
Scramble
PGAM ASO
H
IKZF2 Intron-2 Methylation
FOXP3 5' Upstream
Serine-Free
Serine
Serine+SHIN1
CpG #254
CpG #255
CpG #256
CpG #257
CpG #258
CpG #259
CpG#-238
CpG#-237
CpG#-236
CpG#-235
CpG#-234
CpG#-233
CpG#-232
CpG#-231
CpG#-230
I
Vehicle
3DZA
CD25
FOXP3
77.0%
98.6%
% CD25+FOXP3+ (fold change from vehicle)
Vehicle
3DZA
J
Vehicle
3DZA
Count
75.2%
61.3%
Comp-eFluor 450-A
% divided
Vehicle
3DZA
K
Vehicle
3-DZA
Weight Change
Post-Injection Day